JOURNAL OF CATALYSIS 138, 413–444 (1992)

The Nature of the Iron Oxide-Based Catalyst for Dehydrogenation of Ethylbenzene to Styrene

2. Surface Chemistry of the Active Phase

M. MUHLER, R. SCHLÖGL,[1] AND G. ERTL

Fritz Haber Institut der Max Planck Gesellschaft, Faradayweg 4, D 1000 Berlin 33, Germany

Received January 21, 1991; revised May 18, 1992

The combination of an XPS/UPS surface analysis instrument with a microreactor allowed the investigation of the surface composition of catalysts characterized by varying activities and selectivities. The active surface is a potassium iron oxide with a 1 : 1 atomic ratio of K : Fe, whereby iron is only in its trivalent state. Conversion of oxidic oxygen to OH groups is detrimental to the activity. No significant amount of promotor additives is present in the active surface. The process of regeneration with steam removes carbonaceous deposits but cannot reoxidize iron from Fe^{2+} to Fe^{3+}. A constant but small amount of potassium carbonate that cannot be increased by addition of CO_2 to the feed of the working catalyst is present at the surface. Catalysts are precursors, active materials, and irreversibly deactivated samples were studied by SEM and TEM. The surface morphology as well as the microstructure clearly indicates a solid as the active phase. This phase is generated and maintained through solid-state reactions during operation. A potassium-rich liquid film with a thickness exceeding one monolayer can be ruled out for the catalyst performance. Formation of droplets of KOH in certain regions of the catalyst signals bulk structural desintegration of the active material.

1. INTRODUCTION

The characteristic bulk chemical properties of the essential iron potassium oxide system used for dehydrogenation of ethylbenzene to styrene have been described earlier (*1*). It was found that the catalyst in its active state is a metastable mixture of three phases, namely $KFeO_2$, $K_2Fe_{22}O_{34}$, and Fe_3O_4. Under the influence of the reducing operating atmosphere this mixture decomposes slowly into a thermodynamically stable two-phase system of Fe_3O_4 and KOH representing the irreversibly deactivated catalyst. The process is a solid-state chemical reaction controlled by structural imperfections of the starting mixture, which can be modified by either preparation conditions of the precursor or by the addition of structurally active promotors.

The notorious nonstationary catalytic performance of the system implies that short-term reversible deactivation processes other than the bulk desintegration come into play. The role of CO_2 as catalyst poison and of carbonaceous deposits as site blocking agents has been discussed (*2*) and will be tested in deactivation experiments described below.

Surface analysis of the catalyst faces several problems. The metastable nature of the active material requires *in situ* preparation under technical conditions (873 K and 1 atm of steam) and a suitable rapid transfer technique into the UHV of the analysis system. This problem was solved as described elsewhere (*3*). A second difficulty consists of the inherent insensitivity of the spectral pa-

[1] To whom correspondence should be addressed at Institut für Anorganische Chemie der Universität, Niederurseler Hang, D 6000 Frankfurt 50, Germany.

0021-9517/92 $5.00

rameters of iron oxides to the formal valency. The reason for the insufficient chemical sensitivity of Fe XPS is the open *d* shell valence electron configuration of iron ions giving rise to complex spectral transitions as final state effects which broaden the spectra and cause the appearance of many unresolved structures in the spectra. These effects have been discussed (*4*) in connection with single-crystal reference experiments. The present samples are far from ideal for photoemission measurements and give rise to weak and additionally broadened iron spectra only. Therefore it turned out to be essential to repeat the reference experiments under conditions similar to those of the catalyst data acquisition.

2. EXPERIMENTAL

The catalysts used in this study have been described in the analytical part of this work (*1*). The reference iron oxides were synthesized *in situ* from high-purity iron foil (Ventron), which was sputter-cleaned and subsequently treated with either 500 mbar oxygen or 20 mbar water vapor. The detailed reaction conditions were chosen such that the preparation information from the iron–oxygen phase diagram, which ensured structural identity of the generated thin oxide films with bulk phases, could be used.

The experimental system has been described elsewhere together with some results (*3*). Briefly, a microreactor housing 10 ml of catalyst as a 1-mm sieve fraction is coupled to a UHV system equipped with facilities for XPS, UPS, a gas inlet system, and a quadrupole mass spectrometer. A second sample manipulation system allowed treatment of powders or foils at atmospheric pressures and temperatures up to 900 K. The catalysts were operated continuously for up to 500 h at 873.0 K and at a feed of 1.1 vol ratio ethylbenzene and water. The LHSV was with 0.5 h^{-1}, the same as under technical conditions. Product analysis was performed quantitatively off-line with a gas chromatograph separating the liquid components on a packed column with Bentone on an inorganic support as stationary phase [0.5-μl sample, FID, temperature 383 K]. Qualitative analysis was performed on-line with the quadrupole mass spectrometer coupled to the outlet of the microreactor via a differentially pumped capillary. The reactor is designed such that a fraction of ca. 0.8 ml catalyst placed in a crucible that is fixed inside the reactor bed can be transferred reversibly into a small UHV preparation chamber and then into the analysis chamber. The catalyst sample for analysis was taken from near the center of the reactor bed. From previous studies (*5*) it was known that the top surface of the catalyst bed is not representative of the whole catalyst.

Experiments showed (*3*) that the transfer had to be made such that any contact of the sample with air (even at reduced pressure), pumping oil, or the reaction atmosphere at temperatures below 873 K was strictly avoided. Rapid quenching was achieved by exposing the sample immediately after interruption of the feed to the vacuum generated by a 500 liter/s turbomolecular pump. Within ca. 60 s the sample was cooled to below 500 K and the pressure dropped below 10^{-6} mbar. The subsequent transfer to the analysis position was performed in an all stainless-steel environment. Several transfer procedures were developed to ensure that there was no detectable influence on the sample.

After analysis the sample was usually transferred back into the microreactor and the catalytic testing ws continued. If the analyzed sample was used for bulk structural characterization it also had to be transferred back into the reactor. The latter was then removed as a whole, thus allowing the specimens to be taken simultaneously from the catalyst bed and from the material in the analysis chamber, where it had been possible to expose it, e.g., to an atmosphere different than that of the rest of the catalyst bed.

A VSW (vacuum science workshop) HAC 100 hemispherical analyzer was used for recording the photoelectron spectra. It was

operated at 50 eV pass energy for high-resolution spectra and with 150 eV pass energy for survey spectra. Excitation sources were a twin anode Mg/Al$K\alpha$ X-ray source operated at 150 W power and a Leybold gas discharge lamp for UV He(I) and He(II) radiation. Spectra were accumulated with a personal computer that allowed the data to be processed using standard routines of smoothing (FFT algorithm), background subtraction, integration, and peak fitting.

Scanning electron micrographs were obtained from samples mounted with colloidal graphite on Al stubs. Instruments ISI 60 and Jeol JSM 40 both equipped with EDX were used at 20 kV accelleration voltage. No conductive coating was used. HRTEM experiments were performed with powdered specimen dusted with an Ar jet on carbon-coated grids. A Jeol CX 200 θ instrument with top entry stage was used. Any contact of the specimen with solvents was found to alter the structures observed. Only after prolonged electron beam irradiation (200 kV) was some beam damage observed.

3. RESULTS

3.1. Conversion Measurements

The conversion experiments presented here are not kinetic studies, but are carried out to condition the catalyst sample for surface analysis and to characterize the surface by its catalytic performance.

In Figure 1, typical reaction profiles are shown for catalysts 3 and 4. With cat 3 the technical level of conversion was routinely achieved at 888 K, which is the characteristic temperature in technical applications. After initial activation the levels of by-products benzene and toluene followed the level of styrene production, with short periods of instability. During the initial activation the selectivity for styrene was poor at the beginning and improved slightly within the first 5 h of activation when the conversion rose by a factor of 2. The changing selectivity was found in all catalyst runs, and the timescale of improvement varied with composition of the precursor over an order of magnitude (see, e.g., bottom curves in Fig. 1).

With cat 4 it was difficult to achieve technical steady-state activity. A typical run is shown in the lower half of Fig. 1. Conversion to styrene starts at ca. 15% and increases very slowly over a period of 4 days. Neither temperature variation nor regeneration with steam had much influence on this behavior, which was also found with cat 1 and cat 2. The average activities were ca. 60–70% of the values of technical application under identical synthesis conditions. The difference in activity is ascribed to the large differences in reactor size and design between the technical reactors housing several kilograms of catalyst as 6-mm extrudates and our microreactor containing the test crucible. Small deviations from an ideal gas-flow pattern may have caused deviations from the standard atmosphere and thus influenced the solid-state reactions of catalyst activation. Different types of catalyst proved to be more or less sensitive to these variations. It was not possible, however, to analytically trace back such differences in detail. That means all data presented on the potassium iron oxide system were found to be very similar for all four catalyst samples. Clear correlations between activity and spectroscopic properties were established, however, with one catalyst at different levels of conversion.

In Figs. 2 and 3, reaction profiles of deactivation experiments are presented. Figure 2 shows the effect of a deliberate interruption of the water feed for 15 min simulating a typical breakdown situation of technical operation. The interruption causes a rapid loss of activity by ca. 5%, followed by a period of continuous deactivation. After a total loss of 10%, conversion surface analysis, followed by a regeneration cycle (2 h steam at only 873 K) with immediate subsequent surface and bulk analysis, was carried out.

In this experiment the by-products again follow the trend in styrene production. This observation is in contrast to the microreac-

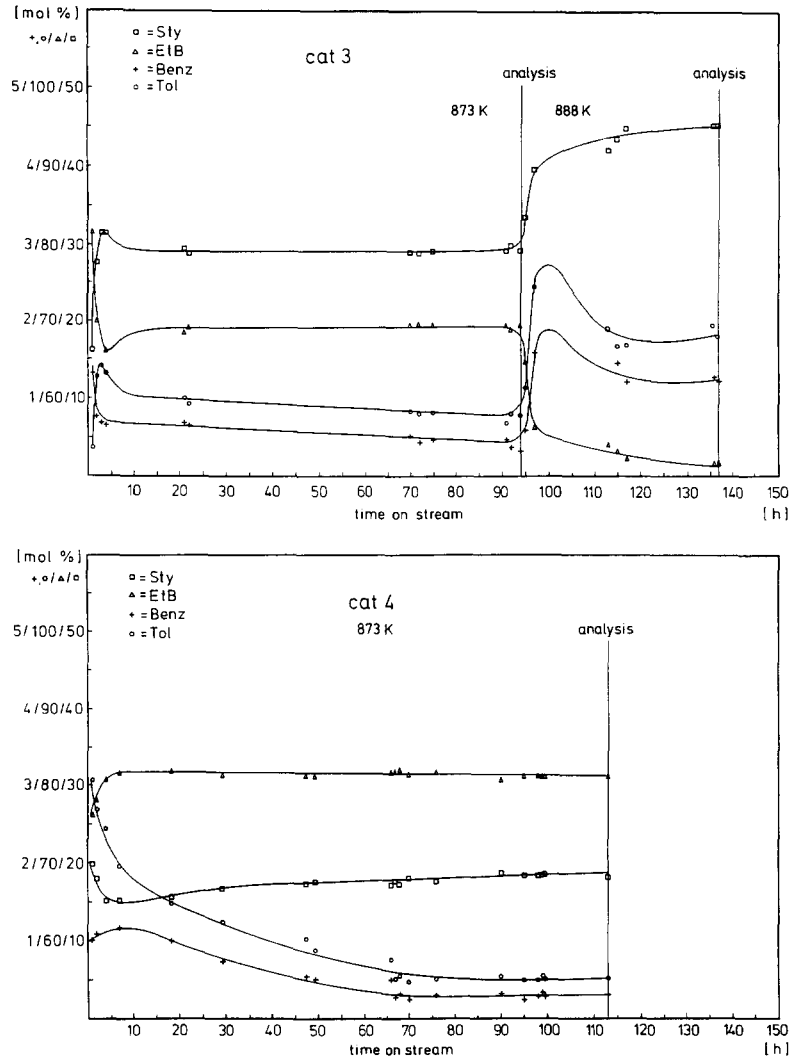

FIG. 1. Conversion vs time profiles for cat 3 and cat 4 in the microreactor. At the points "analysis" the catalyst was analyzed by XPS and UPS.

tor study of Lee (*6*) who reported that a constant rate of synthesis of by-products was independent of the rate of styrene production.

After regeneration no conversion test was carried out since the literature reports that there is a positive effect on the rate of conversion (*7, 8*) which, however, fades away rather quickly and may thus not be detectable analytically after prolonged contact of the regenerated catalyst with the reaction atmosphere. Analysis of the BET surface area and of the lattice constant of the spinel oxide matrix showed no changes in the bulk of the catalyst (see Ref. (*1*), which is in contradiction to the model of Koppe *et al.* (*5*) who found reoxidation of Fe_3O_4 to γ-Fe_2O_3 after regeneration.

The effect of the catalyst poison CO_2 on the reaction profile of cat 3 is shown in Fig. 3. The period of initial activation lasted ca. 45 h, after which surface analysis was car-

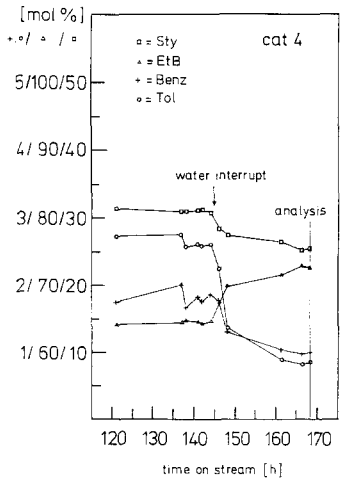

FIG. 2. Conversion vs time profile for a deactivation experiment simulating a sudden change in the partial pressure of water.

ried out. The conversion experiment was continued for 1 day and then CO_2 was added to the feed for 7 h. The amount of CO_2 was chosen to be 0.06 mol/h, as compared with 0.033 mol/h ethylbenzene and 0.22 mol/h water.

Addition of CO_2 caused the styrene production to decline from 41.4 to 16.1%. At this stage, surface analysis was again carried out. After termination of the CO_2 addition, the conversion started to regenerate rapidly, as was also found in a similar experiment carried out by Hirano (*8*). This continued conversion test was performed in parallel with the surface analysis of the poisoned catalyst. After termination of the analysis, the sample was transferred back into the reactor and both fractions of still poisoned and already regenerated catalyst were subject to a structural and BET analysis. Both materials showed the same phase composition of spinel matrix and a small amount of $KFeO_2$ (see Part 1 (*1*); the BET surface areas were, with 2.6 and 3.0 m^2/g (for the poisoned sample), very similar. The isotherms were identical in shape according to their $\alpha - s$ plots, with no indication of pore blocking, e.g., by potassium carbonate, as suggested in the SLP catalyst model (*2*). The XRD phase analysis also gave no indication of the presence of any potassium carbonate phase. It is pointed out that these analyses were carried out under strict exclusion of air from the samples. Air exposure even at room temperature quickly gives rise to the formation of various carbonate phases.

The selectivity increases sharply with the activity step at 20 h and, after a period of unsteady operation, again slightly with the activity reaching its maximum value immediately before CO_2 addition. The activity for by-product formation rises sharply with initial addition of CO_2 and then follows the activity for styrene. From all these observa-

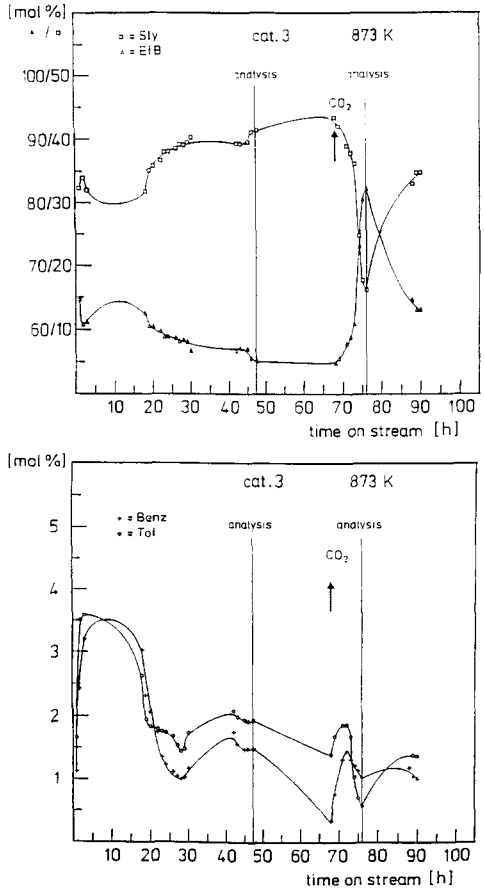

FIG. 3. Conversion vs time profiles for a deactivation experiment with CO_2, which was added (see arrow) for 7 h in twofold excess over ethylbenzene.

tions of the catalyst activity of the by-products, it can be concluded that the hypothesis of Lebedev *et al.* (*7*) and Hirano (*8*) on the existence of a variety of specialized sites for each product is probably correct. The sites that transform the product styrene into benzene or toluene are of the same type and they are different from the sites forming styrene. If these sites are the areas covered with $KFeO_2$, the by-product sites might be those parts of the surface that consist of a Fe_3O_4/KOH mixture; i.e., the selectivity will increase with an increasing surface coverage with $KFeO_2$, or at constant coverage it will decrease with increasing conversion to styrene. The initial improvement in selectivity is thus controlled by the solid-state chemistry of $KFeO_2$ formation; the parallel increase of all organic products with variation of temperature (see Fig. 1) follows from the approach of the main reaction to the equilibrium and the consequently higher concentration of the educt styrene for the side reactions.

3.2. Sample Transfer

This experimental aspect was revealed to be of vital importance for the whole study. In a previous communication (*3*), it was demonstrated that the XPS results for oxygen, potassium, and carbon are significantly different for samples transferred in air from those for *in situ* transferred materials. The surfaces of activated catalysts exposed to air were similar to those of nonactivated samples, whereas activated samples after *in situ* transfer exhibited a characteristic difference in the potassium 2*p* binding energy (BE) and showed much less carbon to be present on the surface. In particular, air exposure caused the presence of a large amount of carbonate carbon to be on the activated catalysts. This signals, on the other hand, the beginning disintegration of the activated catalysts in air as deduced from XRD experiments. The amount of oxygen in the form of OH^- was also larger on the air-exposed sample than on the *in situ* transferred surface.

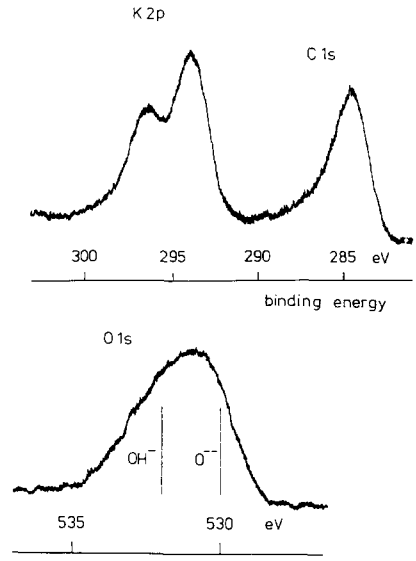

FIG. 4. XPS data for a catalyst surface with the reaction mixture condensed onto its surface. Characteristic are the large amount of hydroxyl species and the abundance of carbon material. See also Ref. (*3*).

If the initial transfer from the reaction atmosphere into the vacuum of the preparation chamber is carried out too slowly, one observes condensation of both the organic phases and water onto the catalyst surface. This effect is demonstrated in Fig. 4 and had to be strictly avoided in the analysis of the active surface, since the unperturbed oxygen 1*s* spectrum contains important information about the active sites (see Section 3.4). The broad oxygen 1*s* spectrum in Fig. 4 is characteristic of a large amount of hydroxyl chemisorbed onto the oxide surface. This surface is covered, in addition, by large amounts of carbonaceous material as reflected by the carbon 1*s* peak at ca. 285 eV.

Another fundamental problem of the catalyst sampling technique is the question of how representative the top part of the content of the crucible is for the whole catalyst surface and how typical is the outer surface of the macroporous material for the internal composition of the catalyst grain. To clarify this, the following two experiments were conducted.

A mechanical device was fitted to the analysis chamber to permit stirring of the contents of the crucible in the analysis position under UHV. Comparison of spectra before and after stirring showed that the surfaces were identical and all grains within the crucible were homogeneous in composition.

In the second experiment, an activated catalyst was analyzed in the conventional way then brought outside the UHV and milled under inert atmosphere into a fine powder. This powder was rapidly reintroduced into the UHV using the fast insertion probe and reanalyzed. The spectral changes were the same as those observed for samples transferred in air. No evidence was found for an increase in the potassium to iron ratio as might result from a pore system in the iron oxide filled with a quenched KOH liquid, such as suggested by the SLP catalyst model (*2*).

3.3. Reference Experiments

Several references deal with the identification of various iron oxides by XPS and supplement the "iron oxide story" written by Wandelt (*4*). Common problems of all iron oxide surfaces are the air sensitivity turning them into hydrous Fe^{3+} oxide and the sensitivity to sputtering leading to reduction into metallic iron. *In situ* preparations can overcome these problems. With the limited pressure ranges of commonly available preparation chambers, however, it is difficult to find reproducible conditions to synthesize well-defined single-phase oxides. In the present work a preparation attachment was designed to allow the synthesis of thin films of iron oxides at atmospheric pressure and at the temperatures used in standard inorganic syntheses (*9*). Under these conditions the nature of the oxide grown on a polycrystalline iron foil (which had been sputter-cleaned and annealed into a well-defined state) is determined by thermodynamics and the iron oxygen phase diagram can be used to define the individual phases (*10, 11*). The oxides were all grown in layers thin enough to avoid electrostatic charging;

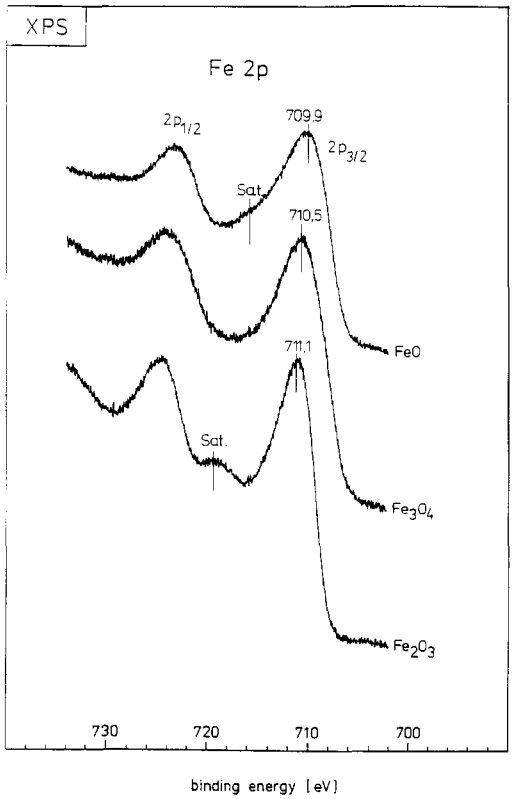

FIG. 5. Fe 2*p* reference spectra for iron oxides prepared *in situ*. The different peak shapes and the visible satellite structures arise from a superposition of many final states involving the open *d* electron valence shell of the iron ion.

i.e., no corrections were necessary for obtaining binding energies of the Fe $2p_{3/2}$ and O 1*s* core levels. Determination of the Fe : O ratio from integration of the core level lines served as an additional check for the integrity of the phases.

α-Fe_2O_3 was synthesized by exposing the iron foil to O_2 at 500 mbar and 773 K for 3 h; the Fe 2*p* BE was 711.1 eV. The corresponding spectrum is shown in Fig. 5. Fe_3O_4 was obtained from exposure of iron to 20 mbar water vapor at 773 K for 10 min with a resulting BE of 710.5 eV. Annealing of Fe_3O_4 in UHV at 873 K resulted in an almost complete conversion into FeO with a BE of 709.9 eV. These data together with the BE of clean α-Fe of 707.6 eV agree well with the literature (*12–14*).

Inspection of Fig. 5 clearly shows that discrimination of a mixture of iron oxides by the BE of the components is not possible, particularly if these are present in widely differing concentrations. The raw data displayed in Fig. 5 further illustrate the problem of subtraction of a suitable background. In this work a step function describing the inelastic energy losses (*12*) as given by Shirley was used. The parameters were chosen such that the fitted background function overlaps with the experimental data at 706 and 730 eV. With this background the spectral intensity remains above zero at all energies between the Fe $2p_{3/2}$ and Fe $2p_{1/2}$ transitions. This intensity is due to the satellite structure arising predominantly from coupling of the iron core hole state with the valence band. These satellites render it difficult to accurately determine iron to oxygen ratios from integration, but can be used for qualitative discrimination of different oxides. In the spectrum of FeO a prominent feature of the satellite spectrum occurs at a distance of 6.0 eV to higher BE from the 3/2 transition: in Fe_2O_3 this feature occurs at a distance of 8.5 eV (see Fig. 5) and in Fe_3O_4 the satellite's feature is absent. These features turn out to be highly reliable indicators of the surface phase composition and can also be used for characterizing mixtures of iron oxides.

The oxygen 1*s* spectra of the three oxides exhibit all the same BE of 529.9 eV. This fact allows use of this BE as an internal standard to correct for charging of the catalyst samples. The oxygen 1*s* profiles were fitted to several Gaussian lines and the component with the absolute lowest BE was set to 529.9 eV. In this way significant charging (ca. 6 eV) was found with the catalyst precursors and with samples exposed to air, but only small corrections had to be applied for the used catalyst materials (ca. 0.2 eV) transferred *in situ*.

All oxygen 1*s* lines of the reference oxides were found to be asymmetric to higher BE. This is illustrated in Fig. 6, showing the smoothed and background-corrected line

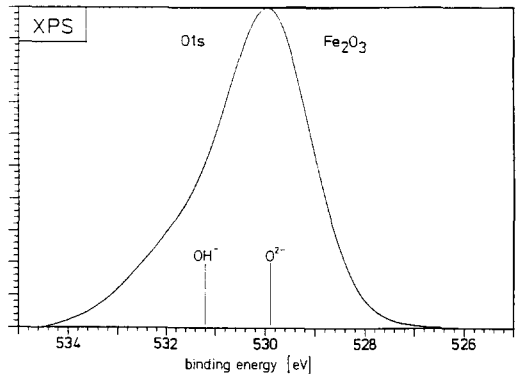

FIG. 6. High-resolution oxygen 1*s* spectrum of *in situ*-prepared Fe_2O_3. The asymmetry to higher binding energy arises from structural hydroxyl. A very small third contribution at still higher binding energy is due to a chemisorbed surface oxygen, which is also identified in the UPS data of Fig. 5 as a shoulder at ca. 3 eV.

for Fe_2O_3. The component of higher BE arises from structural OH present in the oxide. Its fitted BE is 531.2 eV in full agreement with a monochromated XPS study of iron oxyhydroxide showing a resolved OH feature at 531.2 eV (*14*).

To further substantiate the valence determination of the iron oxide surface, ultraviolet photoemission with He(I) excitation was found to be a useful and highly surface-sensitive tool. This technique is difficult to apply to oxide powders as they are generally very poor photoemitters for slow electrons and require analyzer parameters providing only low spectral resolution (ca. 0.5 eV). A set of reference data recorded with these analyser parameters is displayed in Fig. 7. A spectrum from an iron foil contaminated with oxygen is also included. This spectrum is dominated by the iron 3*d* band containing the Fermi edge at zero BE. The spectrum of Fe_2O_3 exhibits zero intensity at that energy in agreement with the insulating properties of this material. The two oxides containing Fe^{2+} ions show a feature ca. 1 eV below the zero energy, which arises from a final state effect characteristic of Fe^{2+} ions (*4*). The dominant feature at 5.5 eV BE in the oxide spectra and the weak structures in the spec-

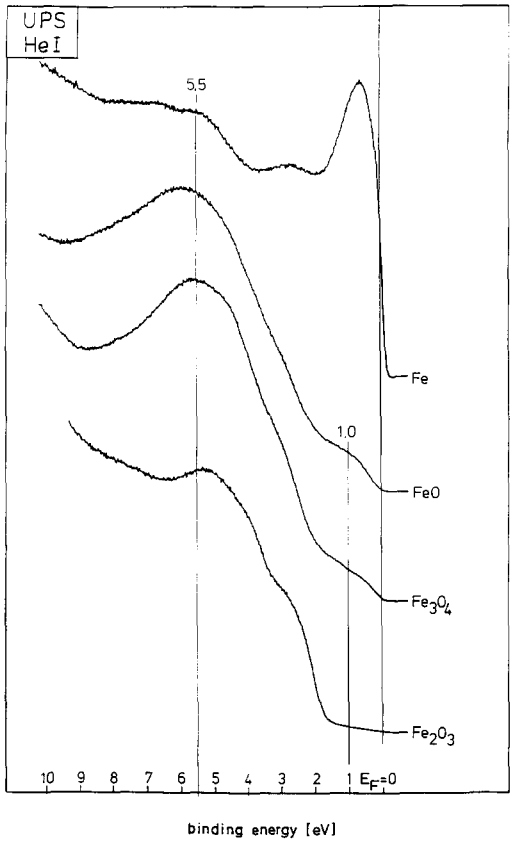

FIG. 7. UPS valence band data of reference materials prepared *in situ*. The structure at 5.5 eV arises from oxygen 2*p* states, and the peak at 1 eV is a final state structure characteristic of Fe^{2+} ions.

trum of the contaminated iron foil arise from oxygen 2*p* states. A more complete discussion of the controversial analysis of the other features can be found in the literature (*15*, *16*).

Reference spectra were also recorded to determine the relevant potassium 2*p* binding energies. KOH was analyzed as a thin film grown from deposition of an aqueous solution on a gold surface kept at 373 K and from subsequent evacuation. The absence of water in the film was verified by the shape and intensity of the oxygen 1*s* line. The K 2*p* BE was found without charging to be 294.0 eV, and the OH^- ions gave a oxygen 1*s* B.E. of 531.7 eV. K_2CO_3 was analyzed as powder after *in situ* treatment with CO_2 at 900 K and 500 mbar in order to remove all basic carbonate. The K 2*p* BE was 293.3 eV with a charging correction, which placed the carbonate C 1*s* BE at 289.9 eV. The potassium ions in $K_2Fe_{22}O_{34}$ also exhibit 293.3 eV BE after the powder sample is annealed in oxygen at 900 K and 500 mbar pressure.

The observed BE for potassium ions compare well with data published by Bonzel and co-workers (*17*). It is noted that the BE of KOH depends strongly on the degree of hydration, with an increased concentration of water leading to lower K 2*p* BE and shifting to below 293.3 eV. This effect is a clear indication of the significant contribution of extra atomic screening to the potassium ion binding energy.

3.4. The Surface of the Active Catalyst

3.4.1. Quantitative aspects. A survey spectrum of the catalyst precursor 3 is reproduced in Fig. 8 and illustrates the typical spectral features of these samples. The spectrum recorded in the constant retarding

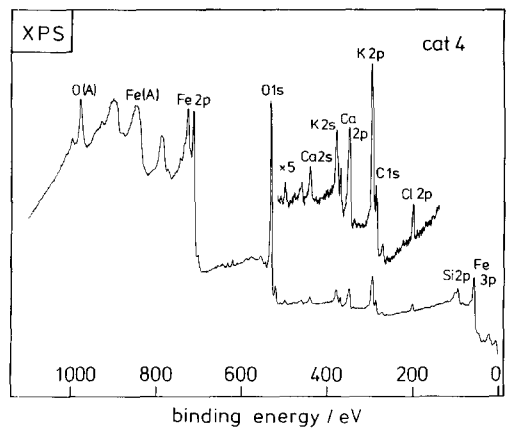

FIG. 8. XPS survey spectrum of the precursor to cat 4. This typical spectrum recorded in the retarding ratio analyzer mode illustrates the surface composition dominated by iron and oxygen and gives an indication for the difficulties with background stripping required for quantitative analysis. The background is even steeper for spectra recorded in the constant pass energy mode.

TABLE I

Surface Compositions of Selected Catalyst Samples in at.%

Sample: Element	Cat 4 precursor	Cat 4 steamed 900 K	Cat 4 after reaction	Cat 3 after reaction
O	40	58	39	45
C	27	8	32	21
Fe	28	25	12	15
K	5	9	13	15
Ca	Not det.	Not det.	2.7	Not present
Cr	Not det.	Not det.	1.5	Not present
V	Not present	Not present	Not present	2.0
W	Not present	Not present	Not present	1.0

ratio mode of the analyzer is dominated by the Auger transitions from iron and oxygen, which also account for the majority of the background electrons. The spectrum illustrates the necessity of a correct background subtraction procedure for obtaining accurate surface atomic compositions. Intense core level features for iron, oxygen, and carbon indicate that the surface is a heavily carbon-contaminated iron oxide. All promotor elements are present in surface concentrations roughly similar to the bulk composition. No significant surface impurities other than carbon were detected in the catalyst precursors.

The evolution of the active surface from the precursor was studied in detail with catalyst samples cat 3 and cat 4 in connection with the activity measurements presented in Section 3.1. The relevant quantitative information obtained from survey spectra recorded in the constant pass energy mode of the analyzer is listed in Table 1. In the precursor, the iron to oxygen ratio is about 1.4 and hence close to the ratio of 1.54 for a ternary oxide with only trivalent iron. After all surface treatments of all catalysts investigated, the oxygen to iron ratio turned out to be significantly larger (ca. 2–1.8) than necessary for any possible oxide composition. This implies the incorporation of hydroxyl in the surface regions. After the reaction, all catalyst surfaces are covered by large amounts of carbon covering the potassium–iron oxides. The structural promotors, however, which were hardly detectable before the reaction, segregate to the surface, indicating the solid-state chemical transformation of the catalyst under reaction conditions. A direct participation of these elements in the catalytic cycle cannot be concluded; however, it may well be that the surface is laterally inhomogeneous and the promotors may be present in islands (see Section 4). The less active catalyst 4 is covered with carbon more severely than the more active catalyst 3, but the oxygen to iron ratio (1.75) and the potassium to iron ratio (1.0) are the same in both samples. A simple correlation between chemical composition of the oxide surface and its catalytic performance was found.

3.4.2. The valency of the iron species. A fundamental question for the reaction mechanism concerns the nature of the iron species in the surface, i.e., the determination of its oxidation state. Only if a significant amount of Fe^{3+} ions is present is it conceivable that the redox cycle Fe^{3+}/Fe^{2+} is important for the mechanism of dehydrogenation. The close-packed structure of Fe_3O_4 does not tolerate any significant amount of excess Fe^{3+} ions, which is, however, known to be present in the active catalyst (*1*). A localization of these excess Fe^{3+} on the surface of the activated catalyst is important to the assessment of the relevance of the catalyst nonstoichiometry activity.

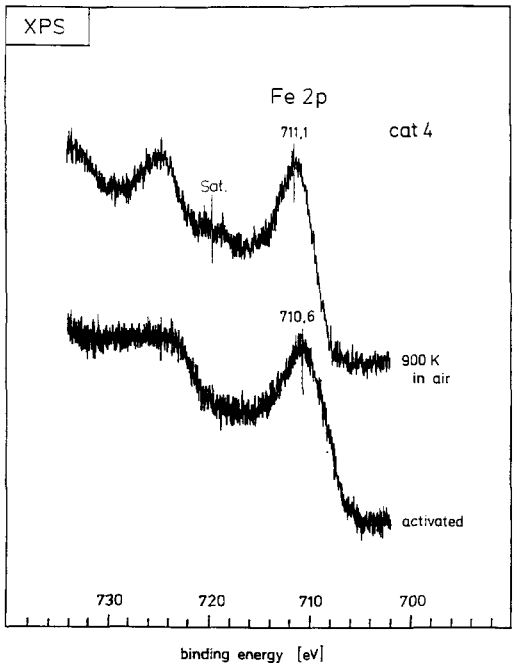

FIG. 9. XPS Fe 2*p* raw data for cat 4 heated in air to 900 K for removal of contaminations and after activation in the microreactor.

In Fig. 9 the high-resolution spectra of catalyst 4 after oxidative heat treatment (virgin catalyst) and after catalysis are compared. Before catalysis the surface consists of Fe_2O_3 characterized by an Fe 2*p* BE of 711.1 eV and a clearly visible statellite. After catalysis the spectrum is more diffuse, the main line has shifted to 710.6 eV, and the hematite satellite has disappeared. This is consistent with a conversion of a large fraction of the surface into Fe_3O_4. The charging of the material was also reduced from 5.0 eV for the unused sample to 0.2 eV for the activated sample, which is in line with the 10^6-fold increase in conductivity upon reduction of Fe_2O_3 to Fe_3O_4 (*9*).

These data show the coexistence of Fe^{3+} with Fe^{2+} on the surface but do not allow quantification of a possible excess content of Fe^{3+} over the stoichiometric amount in Fe_3O_4. This can be achieved using the more surface-sensitive technique of UPS. He(I) spectra of activated catalysts 1 and 3 are displayed in Fig. 10 together with the spectrum of the activated catalyst 1 after oxidation in air at 900 K. The conversion of catalyst 1 was less than half of the conversion of sample 3. It can be seen clearly that catalyst 1 contains a large fraction of Fe^{2+} (feature at ca. 1 eV), which is completely absent in catalyst 3. High-temperature treatment in air leads to almost complete oxidation of the initial Fe^{2+} to Fe^{3+}. This reoxidation does not lead to improved catalytic performance, since the catalyst is very quickly reduced again to magnetite under reaction conditions. This instability of Fe^{3+} in the catalyst surface is correlated with the absence of any structural promotor in this sample.

The spectral features in Fig. 10 are domi-

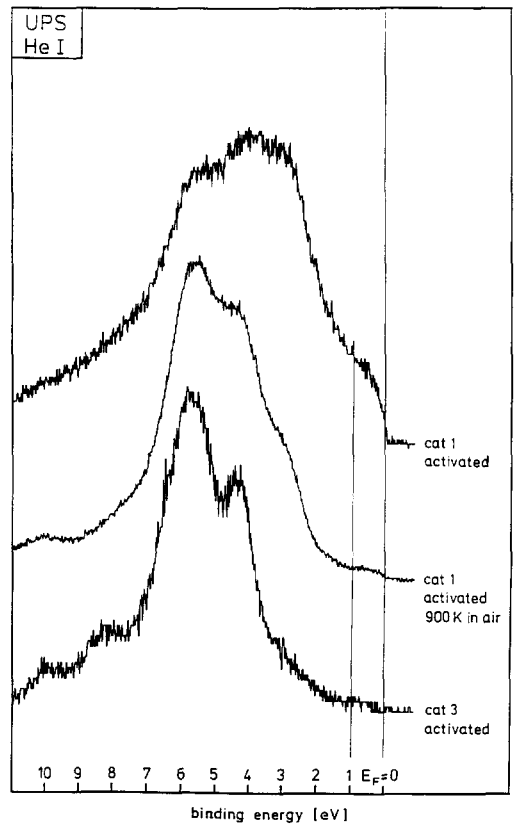

FIG. 10. Valence band UPS data for activated catalysts. These data allow sensitive discrimination between Fe^{3+} and Fe^{2+} (structure at 1 eV).

nated by emissions from oxygen 2*p* states. Exploiting the different trends in cross section modulation of Fe 3*d* and O 2*p* for He(I) and He(II) radiation (*20*), it can be shown that the Fe 3*d* states contribute as a diffuse peak to almost the whole energy range of the spectra shown in Fig. 10. This assignment is in line with discussions in the literature (*15, 16*). Additional peaks at 8, 10, 12, and 15 eV indicate the presence of hydroxyl groups and chemisorbed water (*20*), which is in agreement with quantitative surface analysis.

Activated catalysts with high conversions thus contain a large excess of Fe^{3+} at the surface of a material whose bulk consists predominantly of Fe_3O_4.

3.4.3. The nature of the potassium and oxygen species. Figure 11 summarizes the oxygen 1*s* data in comparison with the potassium 2*p* parameters. The potassium 2*p* spectra of activated catalysts all have the same shape characteristic of a single species with a clear spin-orbit splitting of 2.5 eV. The spectra were recorded after the catalyst samples reached their steady-state conversion at 873 K.

The O 1*s* data contain two contributions that were fixed by line fitting to 529.9 and 531.7 eV and have different relative proportions in all spectra. Using the reference data described in Section 3.3, the main contribution at 529.9 eV is assigned to oxide anions attached to iron; the other species is hydroxyl bound to either iron or potassium. Cat 3 contains a minimum amount of hydroxyl, which is associated with structural OH in the lattice; its potassium is present as potassium oxide as indicated by the low BE of 293.3 eV. All other samples contain anhydrous KOH with a BE of 293.8 eV and consequently exhibit a larger fraction of hydroxyl ions (compare the two spectra of cat 4 with different amounts of potassium). The top spectrum of cat 4 indicates the presence of excess OH in comparison to the potassium content, which should be present as Fe^{3+} oxyhydroxide, since Fe^{2+} hydroxide is a rather labile species.

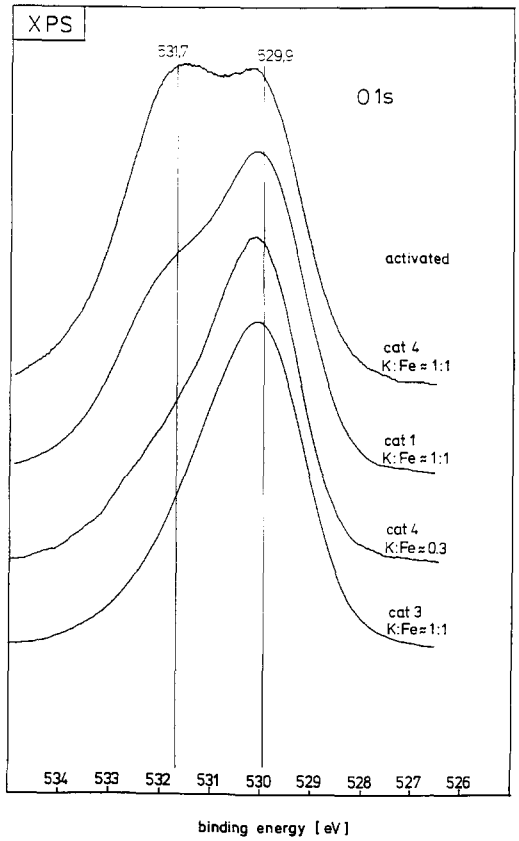

FIG. 11. High-resolution oxygen 1*s* data for various activated catalyst surfaces. The spectra are composed of two components with varying abundance. The positions of the lines were obtained by peak fitting of the four spectra. For comparison of the line profiles with the atomic ratios of potassium and iron see text.

The discrimination between potassium oxide (low BE) and potassium hydroxide (high BE) is possible because of the strong influence of the Madelung potential on the "chemical" shift in potassium XPS (*21*). The positive point change of the potassium ion is more effectively screened by oxide anions (O^{2-}) than by hydroxyl (OH^-). Subsequent replacement of oxide by hydroxyl (basic potassium oxide) leads to a continuous shift in the K 2*p* BE between the limits shown in Fig. 11. This variation was indeed observed in the many spectra acquired during this work.

In summary, the surfaces of all samples

contain several oxide ions bound to iron and varying amounts of hydroxyl ions that belong as structural OH to the iron oxide and as surface OH to potassium as well as to iron oxyhydroxide. The samples contain the anhydrous potassium either as potassium oxide or hydroxide. The presence of thick films or islands of KOH on the unperturbed activated surface can be excluded, since such multilayer hydroxides tend to contain water molecules as structural hydrates, which are clearly absent in the spectra shown in Fig. 11. The broadened profile of the O 1*s* line in Fig. 4 gives an example of partially hydrated KOH. The formation of a possible ternary iron potassium oxide or the presence as a binary phase supported on Fe^{3+} oxide cannot, however, be discriminated by XPS.

3.4.4. Nature of the carbon deposit. All activated samples contain a significant amount of carbon at the surface. This carbon may block active sites, and in industrial practice a steam regeneration cycle is applied to remove this poisoning effect. In order to evaluate the efficiency of this treatment it is important to know the chemical nature of the carbonaceous deposit. It was speculated that it may be present either as graphitic carbon and/or as potassium carbonate (*2, 7, 8*). In Fig. 12 XPS and Auger data of a typical activated catalyst surface are compared with the spectra of a (0001) surface of graphite (highly oriented pyrolytic graphite, cleaved surface).

The BE of 284.5 eV and the asymmetric line profile of the catalyst deposit are in good agreement with graphite reference and were found to be characteristic of graphitic carbon in the literature (*22*). The small peak at BE ca. 6 ev higher in the catalyst spectrum arises from carbonate. The intensity of this peak relative to that of the main line was frequently observed to be variable, which excludes the possible assignment of the small peak to a plasmon excitation of well-ordered (chemically inactive) graphite. The plasmon structure in the reference spectrum was deliberately removed by introducing many cleavage defects during sample preparation.

The valence Auger transition of carbon serves as additional identification for the predominant sp^2 character of the carbon; its characteristic structure and the width of ca. 40 eV arises from the self convolution of the graphite valence band in this transition (*23*). Hydrocarbons would exhibit a much narrower Auger peak with more pronounced fine structure. The peak at 250 eV is due to a potassium Auger transition which obscures slightly the peak shape of the underlying carbon Auger line.

The spectra are good evidence of the predominant presence of graphitic carbon at the surface of activated catalysts with only an occasional minor contribution of carbonate. The carbon likely originating from product polymers is a reactive substrate for potassium-catalyzed gasification by steam in the regeneration cycle (*2,18*).

3.4.5. The structural promotors. The addition of transition metal oxide promotors to the basic catalyst sample cat 1 improves both selectivity and conversion and facilitates the activation of the catalyst to a stable operation. It was shown that these promotors influence the bulk properties of the catalyst (*1*) and it was of interest whether they are also active as surface modifiers.

All these promotors were undetectable at the precursor surfaces unless heated in air to 900 K. Then and after activation, the promotors were present at the surface in amounts corresponding to their bulk concentrations; i.e., under no circumstances was a significant surface enrichment observed.

In Fig. 13 some XPS results are summarized. Chromium is present in the surface of the heat-treated precursor of cat 4 largely as Cr^{6+} (BE 579.6 eV) with a small amount of Cr^{3+} (BE 576.6 eV). After activation the amount of chromium in the surface is reduced and the valency is now entirely +3. This is in agreement with the EXAFS results discussed in Ref. (*1*). The binding energies of the strongest lines of aluminum (2*p*, 73.8

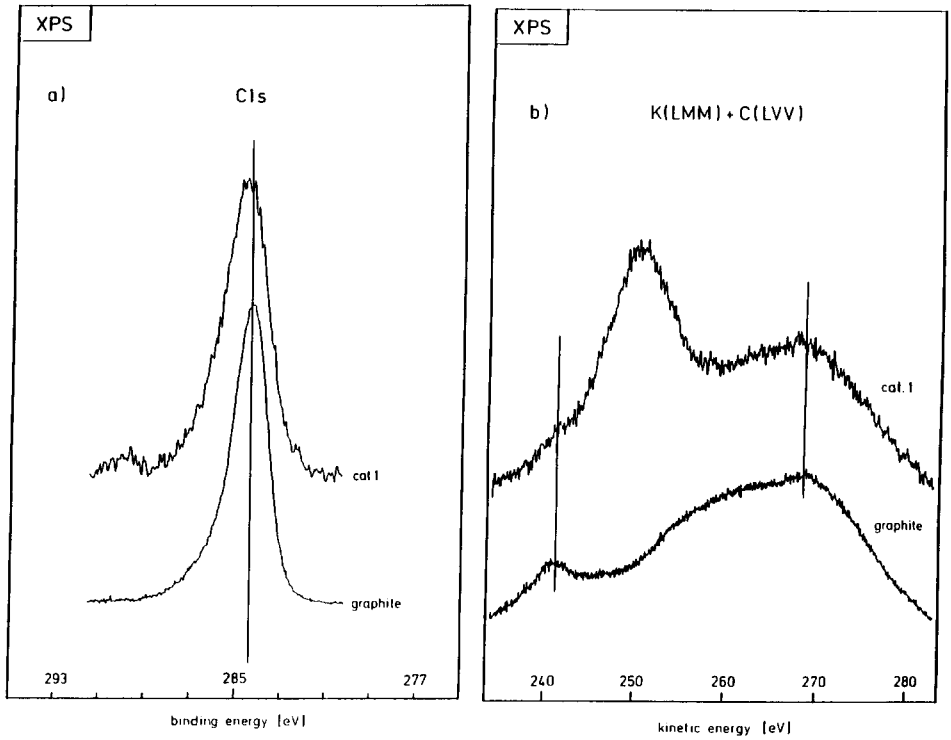

FIG. 12. Chemical analysis of the carbon deposits exemplified with cat 1. Both carbon 1*s* XPS and carbon KLL X-ray-induced Auger data compare well with corresponding data from pyrolytic graphite.

eV) and calcium (2*p*, BE 347.0 eV) indicate the existence of small amounts of oxides in their highest stable formal oxidation states.

The promotors tungsten and vanadium present in cat 3 are also in their highest formal oxidation states (W 4*f*, 35.8 eV and V 2*p*, 517.2 eV). The corresponding binary oxides WO_3 and V_2O_5 are quite susceptible to reduction under conditions of catalysis. It is known, however, that intimate interaction of these oxides with support materials such as alumina (*24, 25*) or formation of tungstates or vanadates (with potassium or iron as counterions) stabilizes these ions against reduction.

In XPS analysis of the promotors there is no evidence of their activity as surface modifiers. The binding energies, which are in good agreement with reference data of oxides (*26*), show the promotors to be present as oxides in their most stable formal valency. It is quite likely that they are all present as ternary oxides embedded into iron oxide, where they exhibit a stabilizing effect against reduction under conditions of catalysis.

3.4.6. Correlation between surface chemistry and catalytic activity. A characteristic behavior of the reaction carried out under technical and laboratory conditions is its unstable operation with respect to conversion and selectivity. It may be speculated that an intrinsic instability of the active surface, which should be detectable with surface spectroscopy, is responsible. Typical situations in which the conversion was found to change significantly are short interruptions of the water feed and temperature shocks and inadequate starting-up procedures which irreversibly damage the catalyst. In many instances a regeneration stop, i.e., steam treatment at reaction temperature,

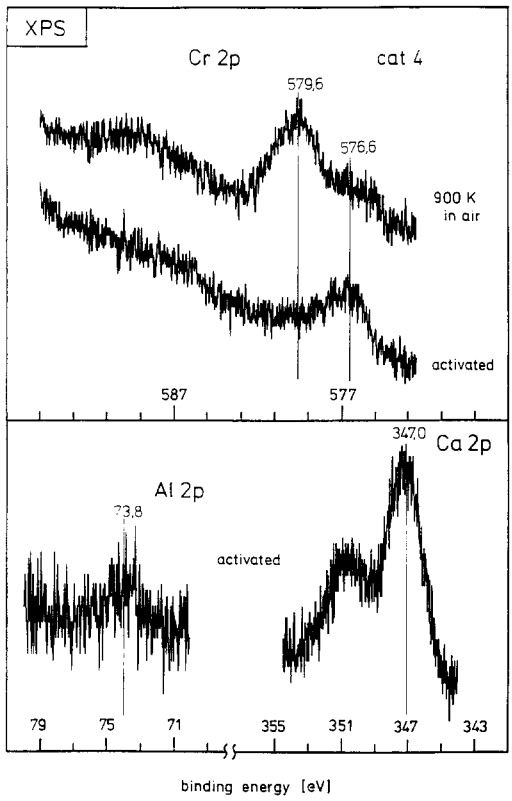

FIG. 13. Selected XPS data for promotor species in cat 4. Only the most intense core levels are nearly detectable (compare also Table 1). No differential charging was observed indicating intimate contact of these oxidic promotor species with the Fe_3O_4 matrix.

leads to a temporary improvement of the performance.

Four hypotheses have been suggested in the literature, namely a change in the ratio of Fe^{3+}/Fe^{2+}, loss of or excess potassium, passivation by potassium carbonate formation, and deposition of large amounts of carbon. A series of experiments with catalyst 3 in which the surface was analyzed by UPS/XPS after a certain level of conversion had been maintained for at least 12 h has been performed. The conversion levels adjusted by varying the catalyst temperature were 17.3, 34.0, 44.9, and 48.2%. The relevant spectral data are summarized in Figs. 14–16.

The ratio of the iron valency is most sensitively tested by He(I) UPS. As can be seen from Fig. 14 there is no significant amount of Fe^{2+} present at the surface, irrespective of the different levels of styrene production. Highly active surfaces contain a significant amount of chemisorbed oxygen atoms as indicated by the peak at 3 eV (*27*), which does not, however, scale with the degree of conversion. These atoms can only be removed by hydrogen reduction or by heating in UHV at 900 K for 12 h. Their presence indicates that a large fraction of the reacting gas–solid interface is indeed of oxidic nature and is not covered by layers of KOH, water, or carbon. The first hypothesis therefore cannot be valid.

Figure 15 compares the potassium and carbon spectra of surfaces with different activities. The selectivities (determined

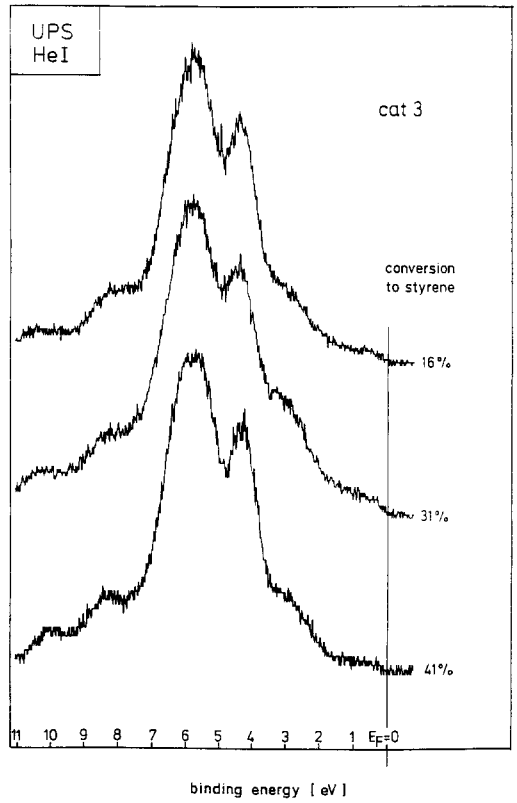

FIG. 14. Valence band UPS data for cat 3 at different levels of conversion. At all levels the surface contains only traces of Fe^{2+} ions (see Figs. 7 and 10).

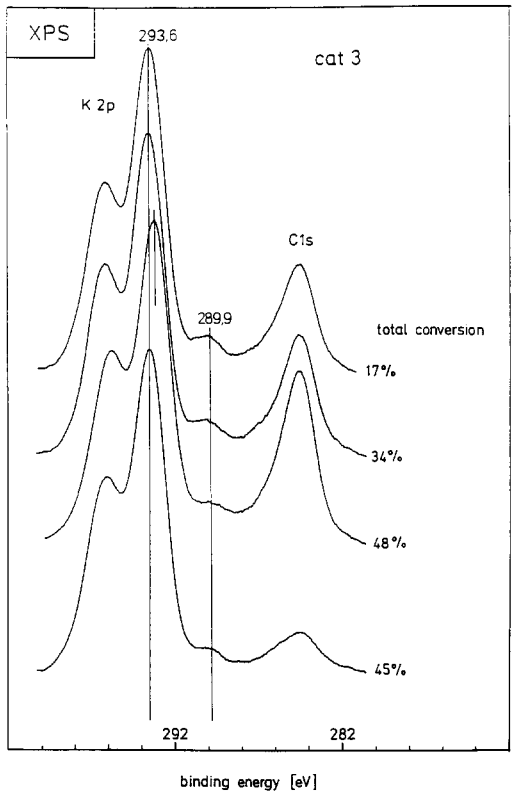

FIG. 15. Potassium and carbon surface species as a function of catalytic activity. The small peak at 289.9 eV is the C 1*s* signal of carbonate.

merely for the liquid products) only range from 90.6% (for 34% conversion) to 93.8% (for 48.2% conversion). The amount of potassium was in all cases the same within 1 at.% and the iron to potassium ratio was 1 : 1 in all cases. Thus, the second hypothesis can also be excluded. All surfaces contain the same amount of carbonate (peak at ca. 290 eV), which excludes the passivation hypothesis. The amount of graphitic carbon is significant but certainly does not supress catalytic activity. From a comparison of the C 1*s* intensities with the UPS data, it turns out that the carbon cannot be present as a continuous layer but must form multilayer islands leaving blank some of the oxide surface containing the iron and potassium ions.

Having excluded all four hypotheses for short-term deactivation, the question arises whether surface spectroscopy samples the active centers at all. Since there is no correlation between the amount of any surface component (including the structural promotors) analyzed so far and the catalytic behavior, the active centers must either have a small concentration or are not located in the parts of the catalyst sampled by XPS/UPS. This latter argument is highly unlikely because of the identity of surface compositions at the periphery and the central parts of the catalyst grains (see Section 3.2).

Moreover, the activity scales with the surface concentration of hydroxyl groups, as seen in Fig. 16. The high-resolution raw data exhibit some asymmetry which scales with

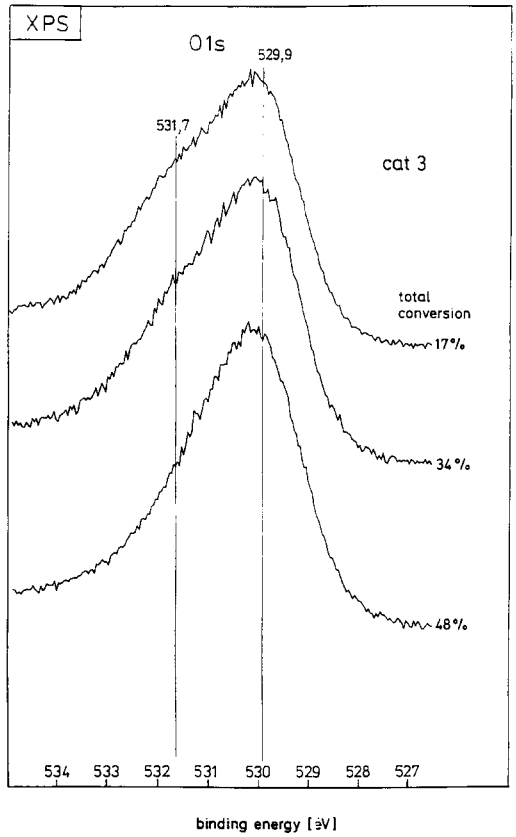

FIG. 16. High-resolution oxygen 1*s* data at different levels of conversion. The integral intensities are normalized but the intensity differences in the raw data were less than 10%. The two lines denote positions found by line profile analysis.

conversion. Line profile analysis was first attempted with two contributions. The line parameters at 529.9 and 531.2 eV were taken from the reference spectrum of iron oxide (see Fig. 6). However, these fits left considerable intensity at higher binding energy unaccounted for, which required the inclusion of a third component located at 531.7 eV. A straight line correlation is obtained between the integral of the high-energy contribution and the conversion. Using the reference data from Section 3.3 the three contributions are assigned to oxide anions coordinated to iron (529.9 eV), to oxide ions coordinated to potassium which appear together with structural hydroxyl groups of the oxide matrix at 531.2 eV, and to hydroxyl groups coordinated to potassium at 531.7 eV. Their presence is detrimental for the catalytic performance. Not KOH but potassium oxide as ternary $KFeO_2$ leads to the most active catalysts. The potassium 2*p* binding energy is also lowest for maximum activity (K–O groups) and increases with decreasing conversion (K–OH groups), indicating the successive hydroxylation of potassium as a consequence of disintegration and/or incomplete formation of $KFeO_2$.

Taking all these data together, a picture of the active surface emerges: On top of a magnetite matrix a layer of ternary oxide $KFeO_2$ is precipitated. It contains only Fe^{3+} and K^+ ions and oxide anions. Part of this surface is covered by graphitic carbon during operation. Irreversible reduction of the ternary oxide caused by fluctuations in the hydrogen–water content of the reaction atmosphere leads to formation of Fe_3O_4 and KOH, which is converted partly into carbonate by the reaction by-product CO_2.

3.4.7. Deactivation experiments. Catalyst deactivation occurs as a long-term process associated with a morphological disintegration (see below) and as a short-term effect caused by irregularities in the feed composition. The short-term deactivation can be reversed by a regeneration treatment with steam (*2, 5, 8*). It has been suggested that the poisoning effect of CO_2 is due to formation of a dense solid layer of K_2CO_3 which would cover the active centers (*2, 5, 8*). The short-term deactivation processes have been simulated in the microreactor, the results of which are displayed in Figs. 2 and 3. The XPS data of the regeneration experiment (see Fig. 2) are compiled in Fig. 17. Interruption of the water feed for 15 min caused the growth of a carbonaceous deposit layer covering the whole surface. Steam regeneration at 873 K caused a large fraction of the carbon to disappear in a gasification reaction likely catalyzed by the potassium present. The oxidic catalyst surface is restored as can be seen, e.g., by the increase of the K 2*p* signal intensity. The gasification does not lead to a significant increase in surface concentration of K_2CO_3; the area ratio between the carbonate C 1*s* peak and the K 2*p* peak remains almost constant. The binding energy of the K 2*p* signal with 293.7 eV indicates hydrated potassium hydroxide species. This was substantiated by X-ray diffraction of a quenched sample of cat 4 after steam regeneration. It consisted of Fe_3O_4 and two additional weak reflections at $d = 2.864$ and $d = 2.689$, which can be assigned to the strongest reflections of $KHCO_3$ and KOH × H_2O. Immediately after regeneration the catalyst does not contain crystalline $KFeO_2$ detectable by XRD. From this analysis it is concluded that a short period for drying up the surface is needed before maximum activity is reached.

In one catalyst literature study (*5*) it was suggested that regeneration leads to reoxidation of iron to trivalent γ-Fe_2O_3. This was not confirmed in precision lattice constant determinations of the regenerated cat 4 (*1*) but a surface layer of only trivalent iron oxide might have been formed. Neither visual inspection nor the difference spectrum of the Fe 2*p* emission line in Fig. 17 gives any hint of excess surface reduction in the deactivated state nor of reoxidation after steam treatment.

The XPS results indicate that feed deactivation for 10 min and successive steam regeneration are associated with growth and

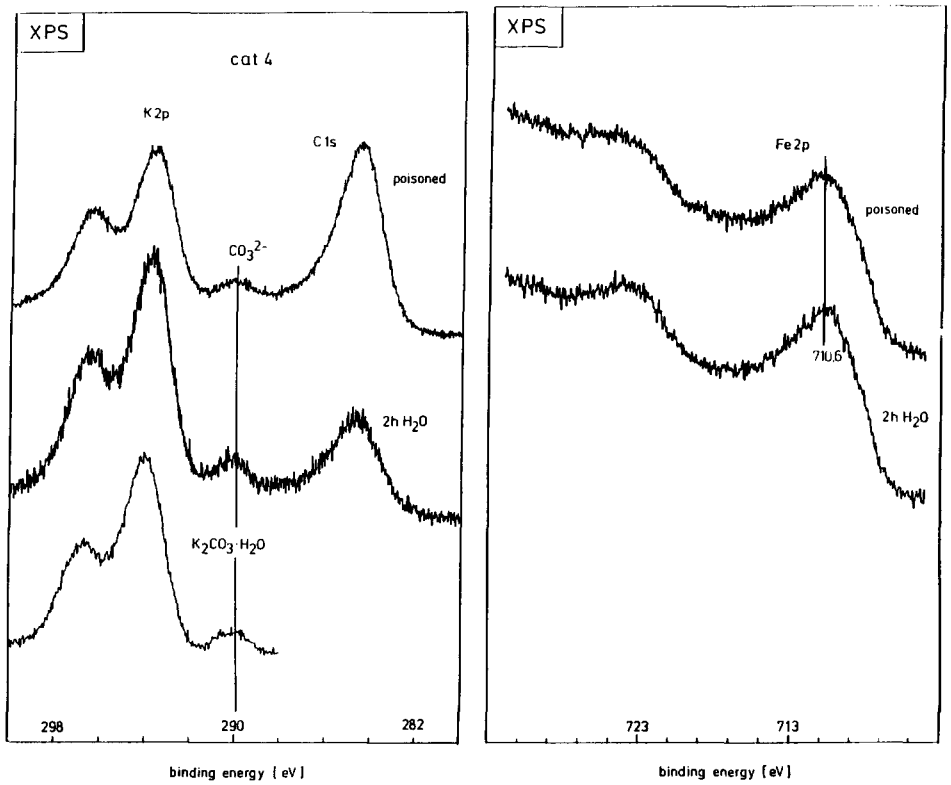

FIG. 17. Surface analysis before and after an interruption of the water feed (see also Fig. 2). The catalyst surfaces were analyzed after the feed interruption ("poisoned") and after steam regeneration ("2 h H_2O"). The spectrum of hydrated K_2CO_3 serves as reference.

gasification of a carbon layer on the oxidic surface. No effects were detected on the iron and on the potassium species present.

The drastic effect of addition of CO_2 to the feed gas on the catalytic activity is illustrated in Fig. 3. A comparison of the XPS data before and after the addition of CO_2 shows that there is virtually no difference between any of the spectra except a greater amount of carbonaceous deposit on the deactivated surface. No indication is found for the formation of a K_2CO_3 layer after dosing CO_2, which is in line with the kinetic observations of Ref. (*8*) whereafter rapid self reactivation of a catalyst poisoned with CO_2 takes place. The blocking effect of CO_2 may be interpreted as competitive adsorption of ethylbenzene and CO_2 at the active centers; given that their chemisorption energies are similar a change in partial pressures will be reflected in the surface abundancies and hence would explain the reversibility of the deactivation after removing CO_2 from the feed. In the present experiments the chemisorbed CO_2 was then lost during evacuation of the sample in the same way that the ethylbenzene is pumped off the surface during the catalyst transfer procedure.

Alternatively the CO_2 may suppress the self-cleaning action of K as gasification catalyst for deposited coke. This could explain the increased abundance of carbon after CO_2 addition and would be in line with the slow response of the system to addition and removal of CO_2.

In summary, the effect on catalytic performance after exposing the catalyst to deactivating conditions, which may well occur

under practical operation conditions, was drastic. The only and reversible effect observed in surface analysis, however, was the increased formation of carbonaceous deposits. No modifications of the iron or potassium species were detected. Steam regeneration is not associated with reoxidation of the iron and does not lead to an increased formation of the active phase $KFeO_2$, which is in line with the stability of the precursor phase $K_2Fe_{22}O_{34}$ against steam treatment (*1*). A direct formation of $KFeO_2$ from the deactivation products Fe_3O_4 and KOH would require oxidizing conditions during regeneration that are not offered by a steam treatment without deliberate or accidental admixture of air.

3.5. Texture and Microstructure

The morphology of the catalyst as precursor, in its active state and after long-term deactivation, was studied in search of potassium films or droplets postulated in the literature and to characterize the microheterogeneity of the material that is relevant to the interpretation of the surface analysis data presented in Section 3.4. On the basis of the information about the micromorphology, an attempt is made to locate the potassium within the iron oxide matrix by high-resolution electron microscopy. The essential results about the location of the potassium have been published previously (*28, 29*) and are only briefly summarized here.

The surface of the activated catalyst consists of a very thin layer in which potassium is highly enriched; using helium ion scattering as a truly surface-sensitive technique, the thickness of the potassium-rich layer was estimated to be about one monolayer. In this layer the potassium to iron ratio is about 1 : 1 in full agreement with the XPS analysis.

Lattice imaging and selected area microdiffraction of a typical platelet structure in the activated catalyst (see below) revealed a spinel lattice of high crystallinity as bulk which is covered by a thin layer (a few unit cells thick) of highly disordered $KFeO_2$. The disorder is seen as an artifact of specimen transfer; under working conditions this layer may be of high crystalline perfection as indicated by the *in situ* X-ray diffraction experiments (*1*). Microdiffraction of the spinel phase revealed that the bulk consists of a solid solution of Fe_3O_4 and $K_2Fe_{22}O_{34}$ in locally varying amounts. An epitactic relationship of the two crystal structures allows for the interpenetration of the two lattices without any mismatch (*1*). The $K_2Fe_{22}O_{34}$ phase is considered the storge phase for two ingredients of the active phase, namely potassium and Fe^{3+} ions.

3.5.1. Catalyst morphology. Figure 18 shows a low magnification image of a cross section of an extrudate from cat 3 after 27 days on stream. The whole cross section exhibits uniform porosity in the micrometer range and some larger voids that are due to manufacture imperfections. Close examination reveals that the granular structure is coarse in an outer ring and more fine in a large central section of the pellet. This effect occurs during operation of the catalyst pellets and leads after prolonged use to physical disintegration of the pellet in an outer shell of brittle character and a dense and hard core separated from the shell by a concentric crack. A preparation of this deactivated state of the catalyst from an industrial sample after 2 years on stream is shown in the inset of Fig. 18 (at half the magnification of the main image). The horizontal streaks are preparation artifacts from the diamond cutting saw.

The materials in the core and in the shell of the catalyst are of different morphology as revealed at higher resolution exemplified in Fig. 19. The core material is made from a dense packing of spherical particles. No pore system besides the intergranular voids can be detected. This is in line with the lower specific surface area of ca. 0.8 m^2/g compared to the fresh catalyst with 2.5 to ca 4 m^2/g (*1*). The shell and the whole bulk of fresh activated catalysts consist of loose stacks of platelets forming a soft and brittle material. The platelets are frequently aggre-

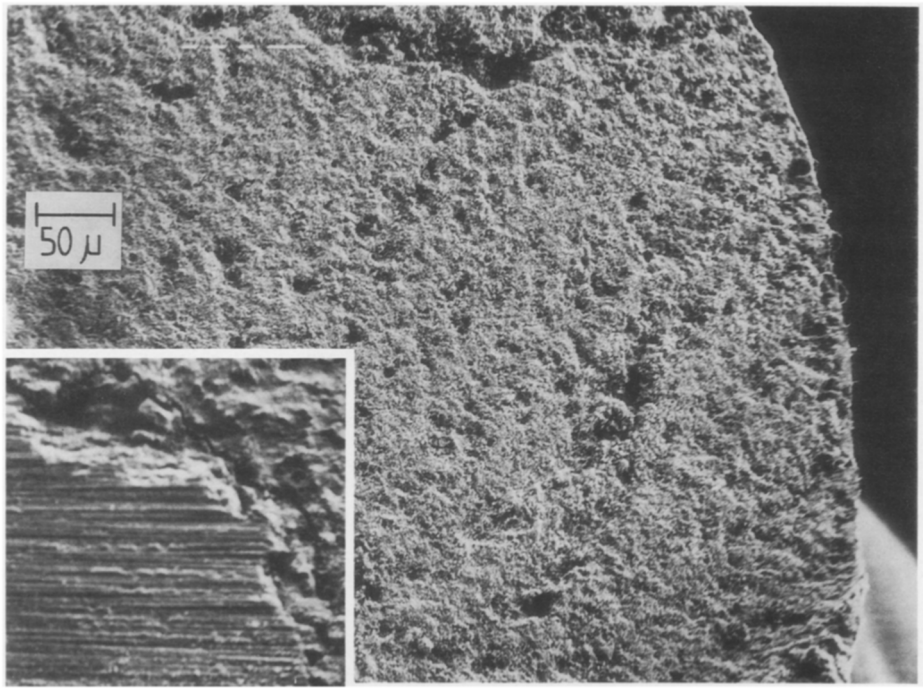

FIG. 18. SEM image of a cross section through a 6-mm extrudate of cat 3 used for 27 days. The inset shows the morphological changes associated with the formation of a core and shell structure. The timescale for this transformation depends strongly on promotion and operating conditions; the image was obtained from a sample after 2 years on stream.

gates of smaller platelets grown on one large base platelet. Typical dimensions range from 0.1 to 5 μm in basis diameter and a few tenths of a nanometer in thickness. This can be seen at intermediate acceleration voltages of ca. 5 kV for imaging which leads to the "soft" contours of the particles in Fig. 19. The inverse video image of a catalyst surface presented in the lower left corner of Fig. 19 reveals the pore system (the dark areas) forming a network of channels for mass transport.

The elemental composition of the two materials is also quite different. Typical EDX traces of a cross section of cat 4 after 1 year on stream in an industrial pilot plant are shown in Fig. 20. The material which is still significantly active exhibits a characteristic gradient in the iron to potassium ratio. The core is enriched in potassium at the expense of the shell. In fully deactivated samples the potassium is only located in the core of the pellets. Promotor oxides are enriched in the shell where they form aggregates of alumina and chromium oxides at the outer surface of the pellet or in large voids. The change in elemental composition is not continuous but occurs sharply in the interface zone indicated by a large crack. Both core and shell are of homogeneous lateral chemical composition except the inner (crack) and outer interface zones. These results are in agreement with data presented in Ref. (*2*) where not only a potassium gradient within a single used pellet is described but also a gradient along the reactor axis with a depleted entry zone and deposition of potassium salts outside the reactor bed. By analyzing a set of seven sections through a 120-mm-long plant reactor it was found that the top 200 mm of pellet bed was almost completely depleted of potassium with

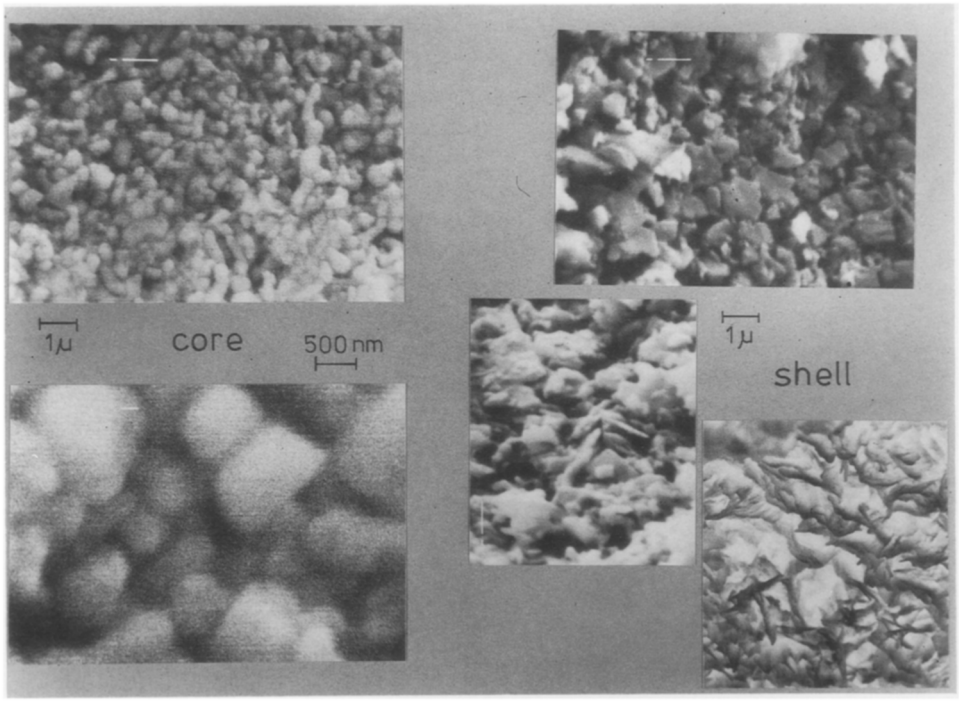

FIG. 19. Typical morphologies of particles in the core and shell region. The bottom left image is reversed in contrast showing the pore system in dark and the catalyst platelets in light.

many pellets being physically disintegrated. The loss of potassium is illustrated by the EDX traces shown in Fig. 21. It turns out that the potassium concentration is affected most strongly by the deactivation process, and the promotors remain largely unaffected in their abundancies. The analyses shown in Fig. 21 for the 700-day sample are taken from almost spherical particles remaining from the original extrudates after gentle touching. Occasionally particles with chlorine contamination can be found in samples run under industrial conditions. The chlorine is located in needles of KCl growing on the outer surface of such particles. In this way some potassium is retained in the original particle but is, most likely not effective in catalysis.

The catalyst samples from the other six zones showed massive core and shell formation with uniform iron to potassium ratios in either core and shell regions. It is concluded that there is no continuously varying gradient in the iron to potassium ratio along the reactor as suggested in Ref. (*2*), but there is a front of complete disintegration of the

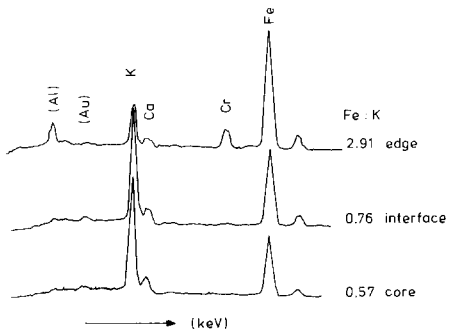

FIG. 20. EDX analyses of particles in the core and shell regions. Excitation was caused with 35 keV electrons over an area of ca. 5 × 5 μm. Tilting experiments excluded absorption effects as explanation for the large variation in potassium content.

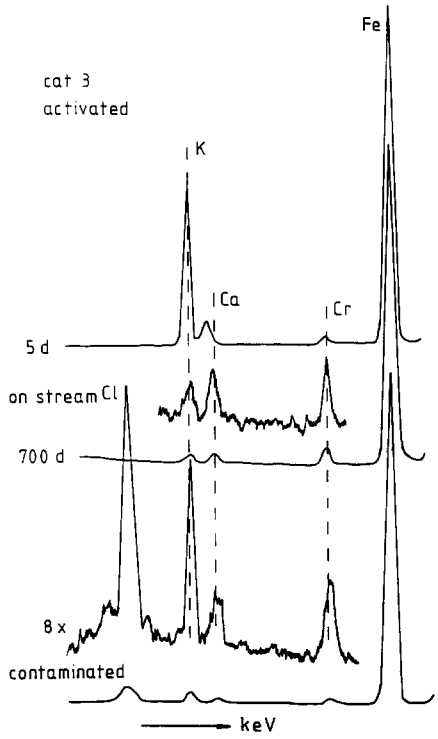

FIG. 21. EDX analyses of samples of cat 3 after various times on stream. Data were taken from fracture surfaces of 1-mm particles for the 5-day analysis and of 6-mm extrudates for the 700-day analysis. Locations close to the outer surface were chosen and analyzed with low magnification (100 ×).

potassium from the iron oxide which progresses through the catalyst bed leaving the rest of the bed unaffected. The depleted potassium is not incorporated into succeeding layers of catalyst but transported out of the reactor. This behavior is in line with the requirement to oxidize some of the iron oxide matrix for excess incorporation of potassium, a process that is not possible during normal operation of the reactor.

The interface between core and shell of a catalyst from sample 4, which had been on stream for 2 months, was prepared, and a view onto the shell side is presented in Fig. 22. The surface consists of patches of a fine granular material rich in iron and large areas covered with a solidified potassium melt. Such images are in accordance with the SLP model which hence holds for the very small volume fraction of the interface between core and shell and describes the deactivated state rather than the operating state of the catalyst.

A pocket in the crack zone in which the potassium melt is located at the core side of the interface is shown in Fig. 23. The elemental analysis of various parts at the shell side exemplifies how the composition is complicated in the interface region. The variation in the Fe : K ratios is free from X-ray absorption effects that were avoided by reorienting the area of analysis into the same geometry of incident beam and detector orientation. The porous nature of the iron-rich oxides allows, however, for some contributions from the potassium-rich background. It can be seen that the Fe : K ratio varies over several micrometers by two orders of magnitude. Four types of objects, namely potassium droplets and three iron oxide species in the form of platelets, needles, and granular aggregates, can be identified. This indicates that the complete removal of potassium out of the platelets leads to recrystallization of the iron oxide, which is a clear sign that the catalyst is undergoing bulk solid-state transformations during operation. The reaction front shown in Fig. 23 is connected with the irreversible deactivation of the catalyst, but was too small in volume to be analyzed by X-ray diffraction. Its location well inside the pellet renders it rather unlikely to exhibit appreciable catalytic activity.

After identification of several nontypical features in the activated catalyst, the typical morphology is now presented in Fig. 24. In this figure the loose stacks of platelets with large and small particles can be identified. The sharp and well-developed crystal edges exclude the existence of a continuous film of solidified potassium melt on their surface. An estimate of the thickness of such an imaginary film from the total amount of potassium and the BET surface area would yield a value of 10 nm, which can clearly be ruled out from the resolution of images as

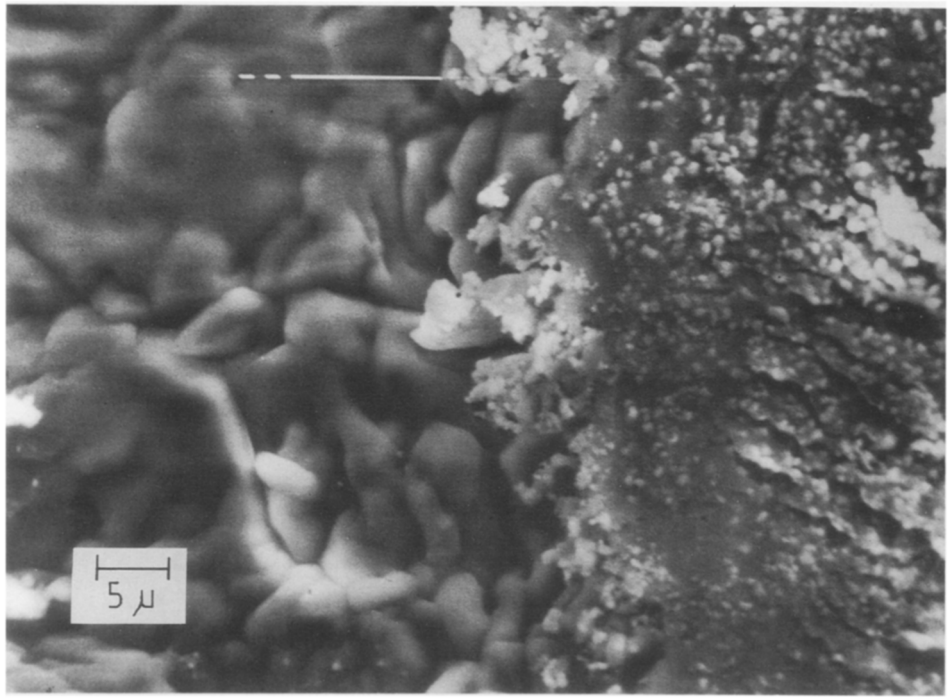

FIG. 22. SEM image of the interface region between core and shell.

shown in Fig. 24. EDX indicates that all particles contain potassium in similar abundancies.

Further strong indication that the potassium is indeed located within the platelets is provided by their morphology. In a control experiment the precursor iron oxide pigment was transformed by thermal treatment within the *in situ* X-ray diffraction camera (*1*) into magnetite. The resulting morphology, which is very similar to that of the starting material, is shown in the inset of Fig. 24 (with half the magnification as the main image). It is thus the presence of potassium that transforms the needles of the precursor material into the platelets of the catalyst. This is in line with the observation of needles in the core and shell interface where potassium-free iron oxide is found. This morphological effect is not systematically influenced by other promotors, the shape and size distribution depends, however, strongly on the iron oxide precursor. Control experiments with several commercial iron oxides of unknown specification gave rise to larger platelets with less structural perfection and locally varying potassium contents.

3.5.2. Microstructure of the activated catalyst. Several activated catalysts from cat 3 and cat 4, after both industrial application and microreactor testing, were subjected to examination in a high-resolution transmission electron microscope avoiding contact of the specimen with both air and solvents. The images presented here complement those published previously (*28*).

Figure 25 shows typical cross sections with the projection axis perpendicular to the basal plane of the platelets. The (311) lattice fringes of the spinel phase can be identified and the layer of $KFeO_2$ can be characterized by its (022) fringes. The image arises from a stack of several very thin platelets with curved edges. Each platelet carries the $KFeO_2$ layer. The top of the image repre-

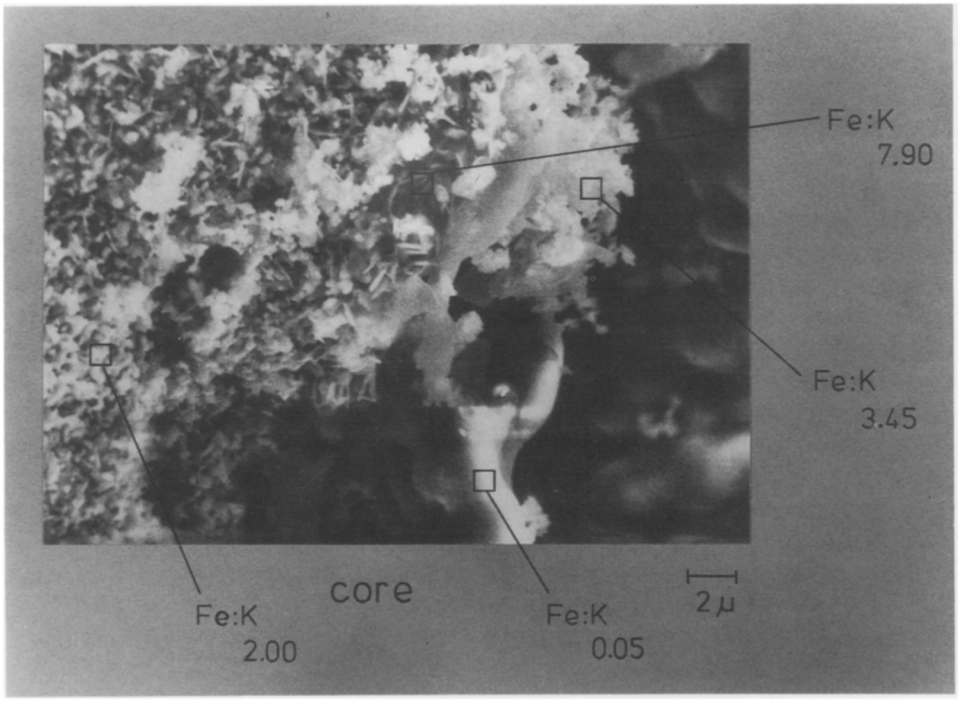

FIG. 23. Elemental speciation for the interface region. The Fe : K ratios are averaged over several point analyses and represent only a trend in compositon due to unavoidable interference and absorption effects in the rough sample.

sents a sequence of terraces and steps on a single platelet as can be concluded from the continuous (311) lattice fringes. Each platelet is a single crystal but contains stepped basal planes which are decorated by $KFeO_2$.

The adlayer covers uniformly and entirely the curved edges by forming microcrystals of ca. 5 by 5 unit cells. The frequent interruption of the lattice fringes of the bulk is due to patches of the $KFeO_2$ layer grown on the basal faces of the platelets. Ordering and thickness of the layer varies from platelet to platelet, as can be seen from a comparison of the main image and the inset of Fig. 25 and also from the micrographs shown in Ref. (*28*). In the inset picture two platelets are stacked onto each other. One of them is thin enough that a focal condition was found for imaging the lattice fringes of both particles. One platelet that is free of the $KFeO_2$ adlayer is a single crystal of $K_2Fe_{22}O_{34}$. The other particle carrying the adlayer is a mixture of $K_2Fe_{22}O_{34}$ and Fe_3O_4 as can be seen from the alternating contrast (period 1 by 1 for Fe_3O_4 and 1 by 2 for $K_2Fe_{22}O_{34}$) in the lattice fringes.

Apart from the contrast from overlapping platelets and from the adlayer on the basal faces there is shallow contrast in all catalyst images running in waves parallel to the crystal edges (see inset of Fig. 25). Neither focus series nor tilting experiments showed step features as the origin of this contrast. It is ascribed to a local variation in chemical composition resulting from reaction fronts of varying potassium content in the iron oxide matrix.

Figure 26 presents a top view onto the basal plane of a thick platelet. The patchy contrast indicates a nonuniform coverage with $KFeO_2$. The dark areas might be covered, whereas the light areas represent the free spinel surface. No indication from im-

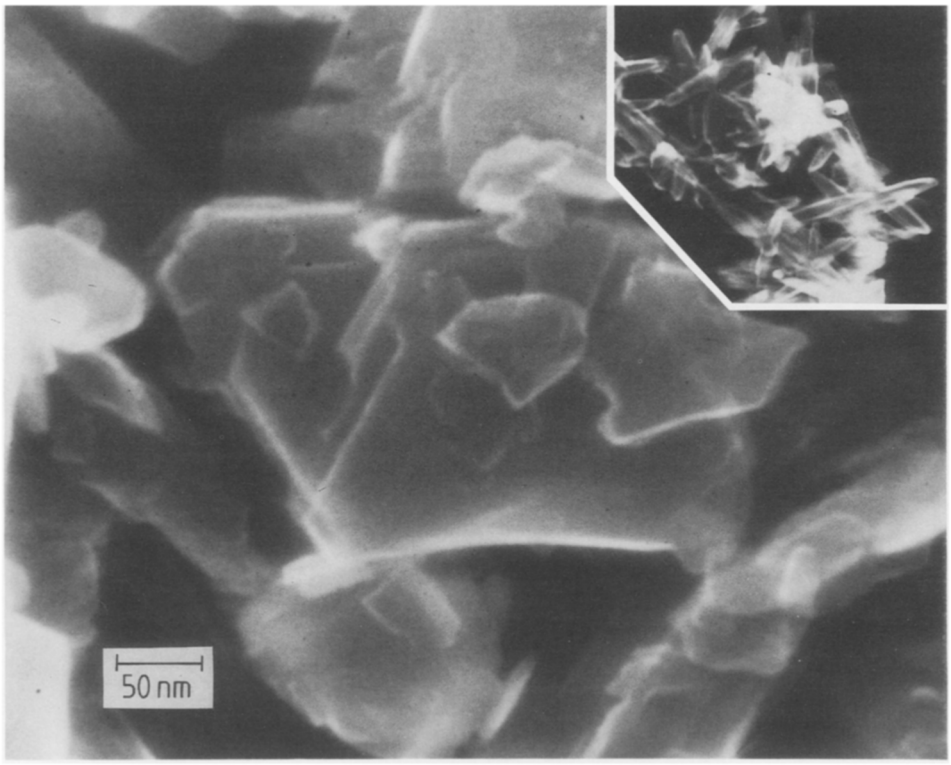

FIG. 24. High-resolution SEM (200 keV) of the particles of an activated catalyst. The inset shows the morphology of magnetite obtained from activation of the pure iron oxide precursor without addition of potassium.

aging or from diffraction was found that carbon deposits cause any detectable contrast. Under the additional assumption that this distribution is not a transfer artifact, the image is an indication that care must be given to the quantitative interpretation of the photoemission results: While the catalysts were uniform on the scale of morphological images, this Figure reveals surface heterogeneity on the microscopic scale, which, of course, is averaged by the photoemission analysis.

The internal structure of a single platelet is imaged in a basal plane projection in Fig. 27. It shows a section of a perfect single crystal with parallel fringes. The decrease of contrast of the fringes within some regions is due to the $KFeO_2$ adlayer, the contrast of which interferes destructively with the bulk lattice fringes. A characteristic feature of the fringes is that the contrast of every second line changes in some regions from light to dark, giving rise to areas with an apparent 1 by 2 sequence and areas with the expected 1 by 1 sequence. Microdiffraction patterns from such areas are similar to those presented in Ref. (*28*) and we attribute this effect to the epitactic interpenetration of the lattices of $K_2Fe_{22}O_{34}$ and Fe_3O_4. The image of Fig. 27 is a projection in the [011] zone of the spinel structure and in the [200] zone of $K_2Fe_{22}O_{34}$. The parallel fringes are assigned to the (311) plane of the spinel structure and to the (010) plane of the ternary oxide structure. The image shows the continuous intergrowth of the potassium storage phase into the iron oxide matrix.

The penetration of potassium into the spinel matrix was studied in a reference experiment. The material $K_2Fe_{22}O_{34}$ was synthe-

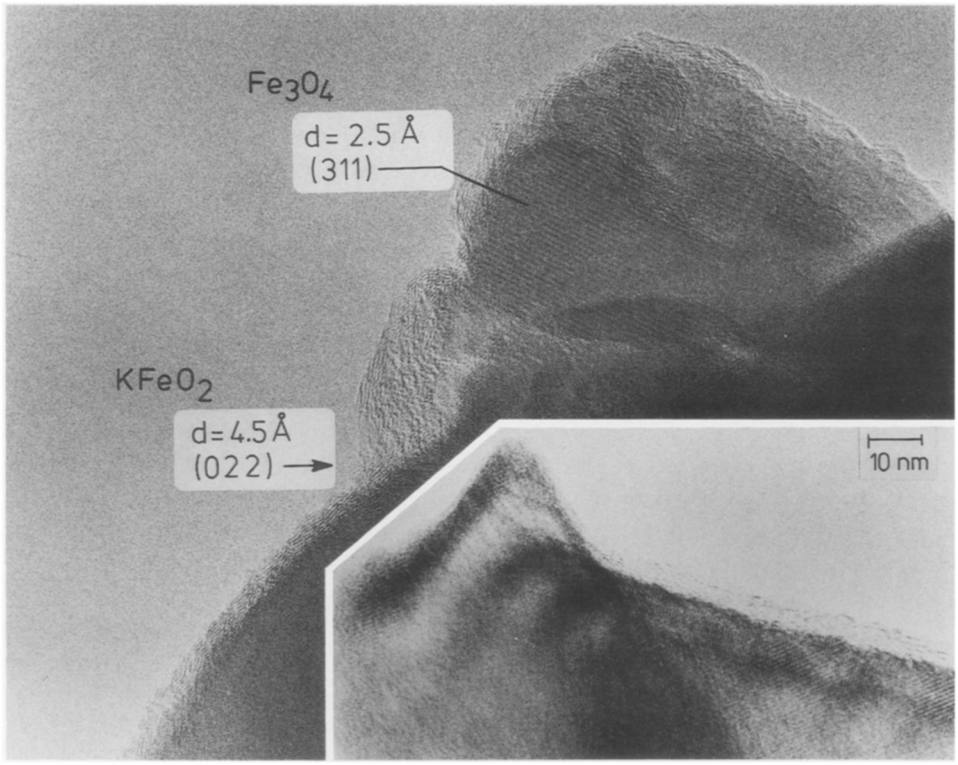

FIG. 25. TEM of activated catalyst particles. The *d* spacings of the lattice fringes were measured from optical Fourier transforms of the image. The inset exemplifies the variation in local composition of the platelets.

sized from Fe_2O_3 and K_2CO_3 at 1200 K according to Ref. (*30*). Powder X-ray diffraction verified the identity of the material. Its morphology showed hexagonal platelets and was very similar to that of the catalyst. Despite the phase purity (as checked by XRD) the potassium to iron ratio varied significantly over a single platelet and between different platelets. High-resolution images of this material in [011] projection revealed the same 1 by 2 contrast variation as with the catalysts samples. An image in the [100] projection is presented in Fig. 28. A well-ordered single crystal of Fe_3O_4, as characterized by two orthogonal sets of lattice fringes, is partly penetrated by potassium. The structure of $K_2Fe_{22}O_{34}$ is in this projection indistinguishable from that of the matrix. The local variation in contrast is in line with the variation in the elemental Fe : K ratio. The image implies that the reaction of K ions with iron oxide is a topochemically controlled process. Its kinetics will hence depend strongly on the texture and grain structure of the precursor iron oxide. All impurities that can pin defects in the parent structure will also influence the progression of the potassium penetration which is only possible in the presence of Fe^{3+} ions in the lattice.

4. DISCUSSION

Now an attempt is made to develop a model for the catalyst operation from a combination of the results presented in the first part of this work (*1*) and in the present paper.

Surface analysis of operating catalysts re-

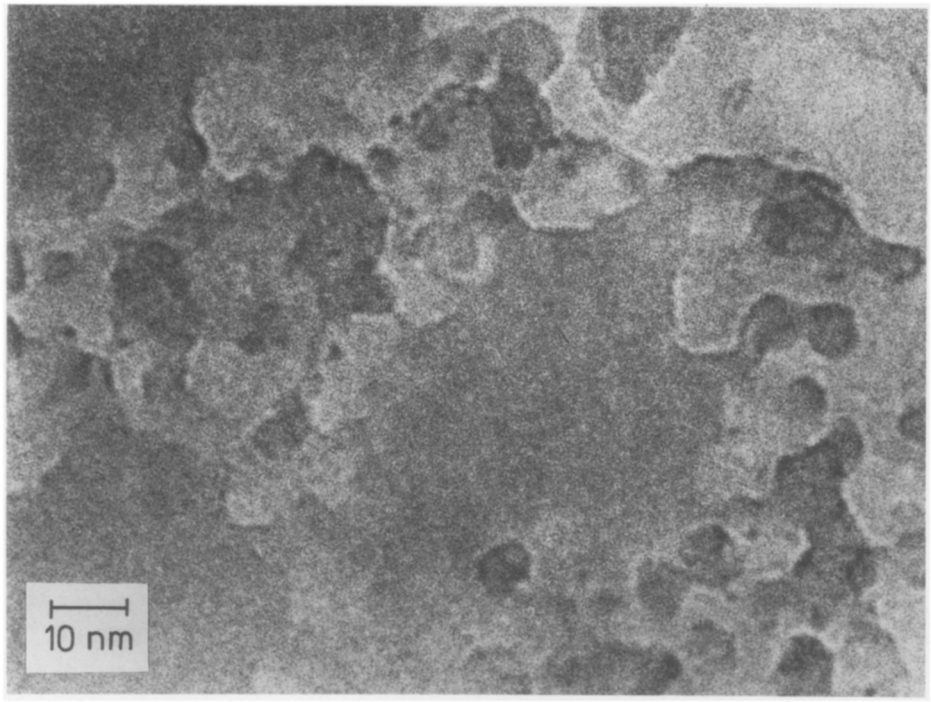

FIG. 26. TEM image of the basal face of an activated catalyst platelet.

veals that the active surface consists of Fe^{3+} and K^+ ions in an atomic ratio of 1 : 1 and of O^{2-} ions. To reach high activity, the amount of OH at the surface must be kept as small as possible. The surface concentration of the promotors is small and most likely they do not directly take part as active centers in the catalytic process. Surface coverage with carbon can vary significantly without greatly affecting the activity. The deposits are of graphitic nature. The catalyst poison CO_2 reversibly blocks surface sites but can be removed by evacuation at 300 K. No excess formation of potassium carbonate is observed. However, all surfaces do contain potassium carbonate but its abundance is not correlated to the catalytic performance.

Reversible deactivation by feed instabilities leads to significant carbon deposition which can be removed by steam regeneration. No effect of this treatment is observed on the valency of the iron; i.e. there is no reduction during deactivation and no oxidation during regeneration. These statements are valid only for relatively short periods of feed instabilities.

The activated catalyst exhibits a characteristic morphology. A macropore system is composed of irregular stacks of hexagonal platelets which frequently appear as aggregates of large and small platelets stacked with their basal planes. This morphology is formed under the influence of the potassium in the precursor state from a variety of other platelet or needle morphologies. After activation the chemical composition is homogeneous.

After less than about 1 month on stream the homogeneous pellet starts to disintegrate into a hard core and a soft shell. In the final stage of catalyst disintegration the extrudate falls apart into powder and hard spherical particles. The core and the shell are separated by a concentric crack in the pellet, which contains the reaction zone. The conversion of the shell into the core

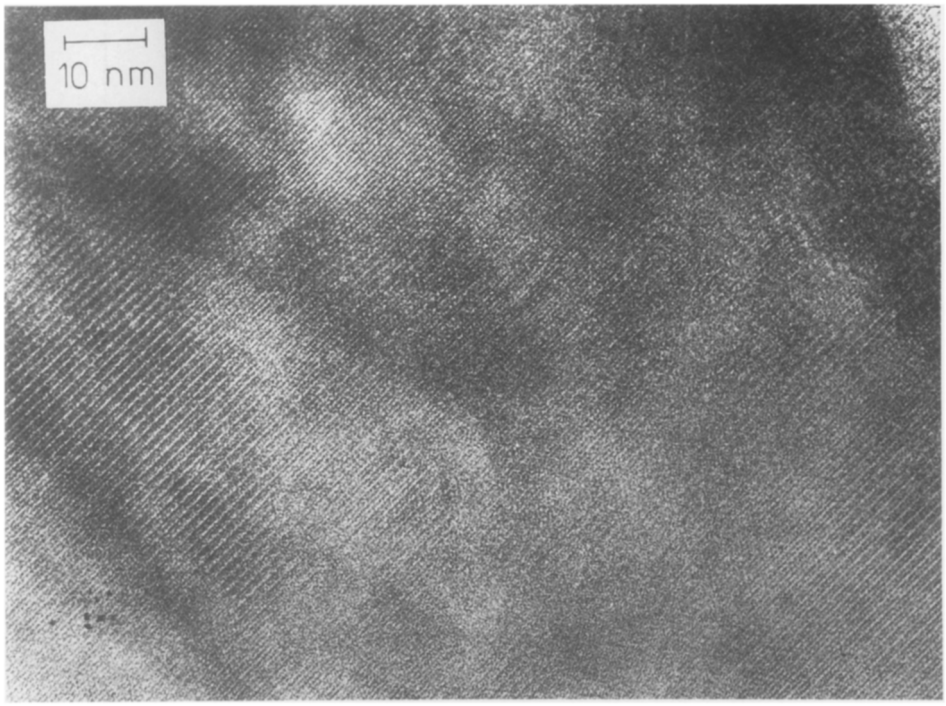

FIG. 27. TEM lattice fringes from an activated catalyst platelet. The periodic variation of contrast in different areas is due to the interpenetration of two phases.

material involves phase separation into a potassium phase liquid at reaction conditions and into several morphologically different iron oxide species. In the course of this deactivation process, potassium is enriched in the core zone and the promotors segregate as particles onto the outer surface of the shell. The final disintegration of core and shell is associated with a total loss of potassium. Occasionally potassium is fixed to the deactivated catalyst in the form of KCl needles. The SLP model of the catalyst describes merely the zone of deactivation.

The microstructure is formed by platelets that are well-ordered crystals of a solid solution of $K_2Fe_{22}O_{34}$ in Fe_3O_4. The surface of these platelets is densely but not uniformly covered typically by about five monolayers of $KFeO_2$, which shows up in the electron microscope as highly disordered material. The ternary oxides contain Fe^{3+} ions exclusively and can only form if not all of the starting material Fe_2O_3 is reduced to Fe_3O_4. Since it has been shown that $KFeO_2$ is the active phase in catalysis, the nature of texture and defects in the starting iron oxide and the kinetics of its transformation into Fe_3O_4 present the key to the catalytic activity of the system.

The reduction of the Fe_2O_3 to Fe_3O_4 is a principally undesired process which occurs, however, for thermodynamic reasons under the conditions of catalysis:

$$Fe_3O_4 + H_2O \rightarrow \alpha\text{-}Fe_2O_3 + H_2.$$

From its $\Delta G = 80.3$ kJ/mol, an equilibrium constant of 10^{-5} at 900 K is derived (*31*). This thermodynamic limitation implies that significant concentrations of Fe^{3+} ions can only exist because of kinetic hinderance of its reduction. Unfortunately, no thermodynamic data for the ternary oxides exist, but it is apparent that the bulk amount of residual Fe^{3+} which allows the formation

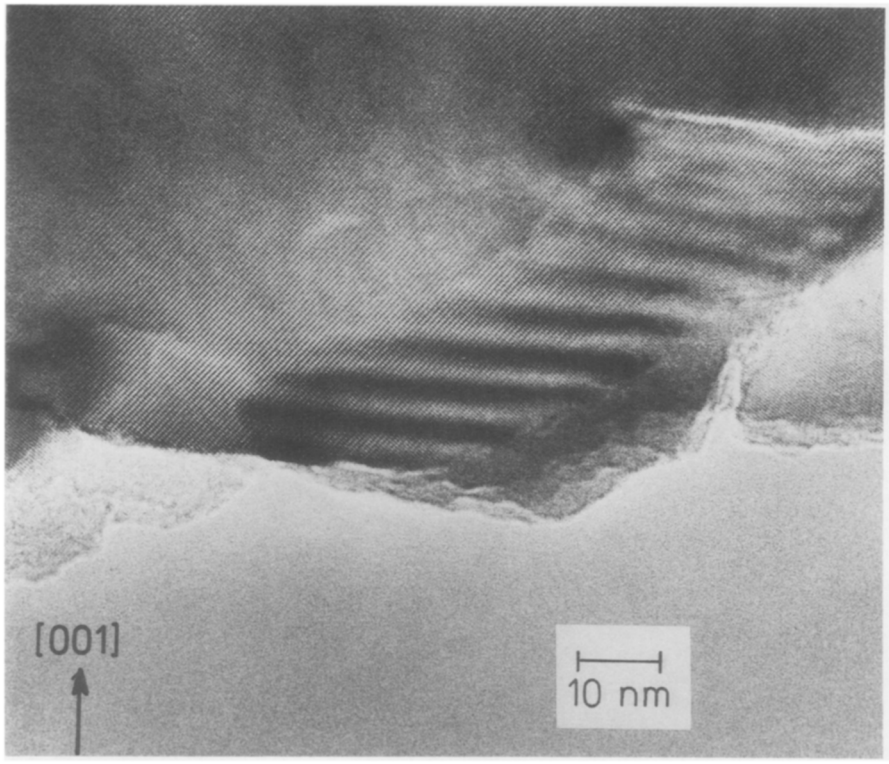

FIG. 28. TEM image of a platelet of iron spinel reacted with potassium carbonate.

of the ternary oxides is thermodynamically instable. The dependence of the catalytic effect of the material on kinetic parameters is the inherent reason for the instability of the catalyst performance.

Thermodynamics of the catalyst further require dilution of the organic feed with steam. If the partial pressure ratio of steam to hydrogen drops below ca. 2 then Fe_3O_4 is fully reduced to metallic iron.

The processes of reduction will be influenced by the presence of potassium. The metastable nature of $KFeO_2$ renders it unlikely that coupling of the iron oxide equilibrium with the formation of this compound has any significant effect; coupling with the formation of $K_2Fe_{22}O_{34}$ which proved to be fairly stable under catalysis conditions (*1*) may stabilize the amount of Fe^{3+}. In this case the stability of the active catalyst will depend on the amount of potassium capable of forming ternary oxides. The equilibrium

$$K_2CO_3 + H_2O \rightarrow 2KOH + CO_2$$

with $\Delta G = +100.0$ kJ/mol at 900 K (*31*) is strongly in favor of chemically bonded (inactive potassium under reaction conditions. This is reflected by the continuous presence of some carbonate at all active surfaces. Short-term exposure to CO_2 does not increase directly the amount of K_2CO_3 because of the absence of free KOH, but it destroys the structural integrity of $KFeO_2$ (*1*), which as a consequence will lead in longer timescales as used in the present poisoning experiment to reduction of the iron oxide, liberation of KOH, and finally formation of K_2CO_3. It is thus essential to load the catalyst precursor with as much potassium stored within the iron oxide as possible in order to have a long lasting supply of chemically active potassium which is not in the form of KOH.

The thermodynamic arguments exclude

also a redox effect on the iron oxide during steam regeneration. This is in line with the XPS data but contradicts the γ-Fe_2O_3 catalyst model (*5*) which also could not be supported by the XRD and Mössbauer results (*1*).

The following scenario for activation and deactivation of the catalyst can be constructed from the information from all the experiments described in this work. The central feature is the formation and disintegration of the active phase $KFeO_2$ (*28*). Formation of this metastable compound requires the availability of Fe^{3+} and K^+ ions within the spinel matrix. Suitable textural properties of this matrix are required to allow appropriate kinetics of the solid-state reaction. These requirements are defined by constitution and treatment of the catalyst precursor. Texture and impurities of the starting iron oxide are of paramount importance since they define the solid-state reactivity of the final catalyst. Addition of promotors may stabilize the iron–potassium oxide materials against reduction by blocking defect sites in the oxide from where the topochemically controlled reduction process starts. The stability of the catalyst precursor against reduction in a dilute hydrogen atmosphere may thus be a suitable test for good catalysts. Good crystallinity of the precursor mixture or a maximum amount of $K_2Fe_{22}O_{34}$ as probed by XRD are not sufficient as optimization criteria since they do not take into account the fact that these are only the starting compounds for a kinetically demanding solid-state reaction. Without a detailed knowledge of the reaction mechanism leading to the formation of $KFeO_2$, very detailed criteria for catalyst optimization are still lacking.

Having reached a coverage of the bulk phase with $KFeO_2$ after some hours of activation several interface and solid-state reactions start to decrease the presence of the active phase. Instabilities in the local or macroscopic partial pressures in the feed initiate several site blocking reactions. If the partial pressure of hydrogen is too high, the Fe^{3+} ions are reduced with the consequence of phase separation of $KFeO_2$ into Fe_3O_4 and KOH. The latter compound blocks other active sites by fixing some hydration water to the surface. Excess CO_2 reversibly blocks active sites by competitive adsorption with the reactant. Excess partial pressure of ethyl benzene causes the formation of carbonaceous deposits that block sites, and in the process of their formation excess hydrogen is produced, which in turn may reduce the active phase. The catalyzed steam gasification generates poisoning CO_2. All blocking reactions that do not reduce the iron can be reversed by steam treatment in the regeneration process.

These interface reactions slowly use up the kinetically stabilized supplies of Fe^{3+} and structural potassium. The end of the catalyst is a "dry" spinel matrix containing only iron as magnetite and the structural promotors which then are accumulated to heterooxide particles. All potassium either has formed stable crystals of K_2CO_3 or has been transported out of the reactor bed.

This state of the catalyst will usually not be reached since another process operating parallel to the interface degradation or initiated by the decomposition products of $KFeO_2$ transforms the catalyst into an inactive state. This process of irreversible long-term deactivation causes the formation of the core and shell structure of the catalyst extrudates. The driving force for this process is the thermodynamic equilibration of the system leading to magnetite and a potassium phase. The reaction comprises a solid-state transformation of the initial spinel iron oxide platelets and the formation of liquid KOH. Morphology and phase analysis (*1*) imply that the process is not a simple one-stage reaction; rather, it seems that several morphologically and structurally different iron oxide species are involved. The transformation starts in the center of a catalyst extrudate and moves in a concentric reaction front towards the periphery. Gradients in either temperature or partial pressures in the extrudate may initiate the equili-

bration which was never observed to form several reaction fronts within a single extrudate. The hypothesis that such gradients influence the equilibration reaction is supported by the fact that the growth of the core is as anisotropic as the outer shape of the extrudate; i.e., the shape of the core is just a smaller image of the extrudate. It was not possible to determine the phase(s) in the core and it is therefore not possible to identify the external parameter that lifts the kinetic stabilization of the initial catalyst material.

It is pointed out that the active phase $KFeO_2$ is also considered to be the active principle in the K–Fe–oxide-catalyzed coal gasification reaction (*32, 33*). This explains the generally small amount of carbonaceous deposits and the self-regenerating effect of the catalyst with steam as dilution agent for the reactant. The nature of the active phase suggests that the elementary steps of the reaction are two proton abstraction processes enabled by a Fe^{3+}/Fe^{2+} redox cycle. Such reactions require strongly ionic catalyst surfaces (*34–36*) providing strong electrostatic fields that induce dipole moments in the chemisorbed organic species and thus lower the activation barrier for the dehydrogenation step. A "naked" potassium ion in the $KFeO_2$ surface will enhance the polarization of a Fe–O bond and increase the basicity of such a reaction center. The presence of hydration water from KOH or of hydroxyl groups coordinated to the iron oxide will lower the polarizing effect and thus reduce the basicity of the reaction center. In this way a correlation exists between the abundance of OH groups at the surface and the catalytic activity becomes plausible.

A more detailed understanding of the reaction mechanism would require a study of the chemisorption properties of the water-free K–Fe^{3+}–oxide surface. On the other hand elucidation of the mechanisms of the solid-state reactions leading to the formation of $KFeO_2$ and to equilibration of the metastable activated catalyst might lead to improvements of catalyst performance and stability.

ACKNOWLEDGMENTS

This work was supported by the Bundesministerium für Forschung und Technologie in a joint project with BASF (Ludwigshafen) and the Universities of Stuttgart and Münster. The authors acknowledge many fruitful discussions with Professors Wicke and A. Bartsch (Münster), Professors Gillessen and M. Zeller (Stuttgart), and Drs. Ambach, Büchele, Hölderich, Mross, and Schwarzmann from BASF. Dr. S. Eder (Munich) conducted preliminary XPS experiments. G. Weinberg (Berlin) and Dr. A. Reller (Zurich) helped in the electron microscopy work. Finally, helpful comments by the referees are acknowledged.

REFERENCES

1. Muhler, M., Schlögl, R., Rayment, T., Dent, A., and Ertl, G., *J. Catal.* **126,** 339 (1990).
2. Mross, W., *in* "Dechema Statusseminar," p.173, 1987.
3. Muhler, M., Schlögl, R., and Ertl, G., *Surf. Sci.* **189,** 69 (1987).
4. Wandelt, K., *Surf. Sci.* **2,** 1 (1982).
5. Koppe, J., Rapthel, I., and Kraak, P., *Chem. Technol.* **40,** 81 (1988).
6. Lee, E. H., *Catal. Rev. Sci. Eng.* **8,** 285 (1973).
7. Lebedev, N. N., Odabashyan, G. V., Lebedev, V. V., and Makorov, M. G., *Kinet. Katal.* **18,** 1177 (1977).
8. Hirano, T., *Appl. Catal.***26,** 65 (1986).
9. Hollemann-Wiberg, *in* "Lehrbuch der Anorganischen Chemie," p. 927. de Gruyter, Berlin, 1976.
10. Kuivila, C. S., Butt., J. B., and Stair, P. C., *Appl. Surf. Sci.* **32,** 99 (1988).
11. Lindner, U., and Papp, H., *Appl. Surf. Sci.* **32,** 75 (1988).
12. Proctor, A., and Sherwood, P. M. A., *Anal. Chem.* **54,** 13 (1982).
13. Allen, G. C., Curtis, M. T., Hopper, A. J., and Tucker, P. M., *J. Chem. Soc. Dalton Trans.*, 1525 (1974).
14. Brundle, C. R., Chuang, C. J., and Wandelt, K. *Surf. Sci.* **68,** 459 (1977).
15. Eastman, D. E., and Freeouf, J. L., *Phys. Rev. Lett.* **34,** 395 (1975).
16. Alvarado, S. F., Erbudak, M., and Munz, P., *Phys. Rev. B* **14,** 2740 (1976).
17. Bonzel, H. P., Broden, G., and Krebs, H. J., *Appl. Surf. Sci.* **16,** 373 (1983).
18. Schlögl, R., *in* "Physics and Chemistry of Alkali Metal Adsorption" (H. P. Bonzel, A. M. Bradshaw, and G. Ertl, Eds.), p. 347. Elsevier, Amsterdam/New York, 1989.
19. Yeh, J. J., and Lindau, I., *Atomic Data Nucl. Data Tables* **32,** 1 (1985).

20. Kelemen, S. R., Freund, H., and Mims, C. A., *J. Catal.* **97,** 228 (1986).
21. Cardona, M., and Ley, L., Eds. "Photoemission in Solids," Topics in Applied Physics, Vol. 1, p. 26. Springer, Berlin/New York, 1978.
22. Schlögl, R., and Boehm, H. P., *Carbon* **21,** 345 (1983).
23. Schlögl, R., Geiser, V., Oelhafen, P., and Güntherodt, H. J., *Phys. Rev. B* **35,** 6414 (1987).
24. Biloen, P., and Pott, G. T., *J. Catal.* **30,** 169 (1973).
25. Grünert, W., Shpiro, E. S., Feldhaus, R., Anders, K., Anthoshin, G. V., and Kh. M. Minachev, *J. Catal.* **107,** 522 (1987).
26. Muilenberg, G. E., "Handbook of X-ray Photoelectron Spectroscopy." Perkin–Elmer Corp., 1979.
27. Kelemen, S. R., Kaldor, A., and Dwyer, D. J., *Surf. Sci.* **121,** 45 (1982).
28. Muhler, M., Schlögl, R., Reller, A., and Ertl, G., *Catal. Lett.* **2,** 201 (1989).
29. Muhler, M., Schlögl, R., and Ertl, G., *Surf. Interface Anal.* **12,** 233 (1988).
30. Scholder, R., and Mansmann, M., *Z. Anorg. Allg. Chem.* **321,** 246 (1963).
31. Barin, I., and Knacke, O., "Thermochemical Properties of Inorganic Substances." Springer, Berlin/New York, 1973.
32. Delanny, F., Tysoe, W. T., Heinemann, H., and Somorjai, G. A., *Carbon* **22,** 401 (1984).
33. Carrazza, J., Tysoe, W. T., Heinemann, H., and Somorjai, G. A., *J. Catal.* **96,** 234 (1985).
34. Gibson, M. A., and Hightower, J. W., *J. Catal.* **41,** 420 (1976).
35. Wang, I., Wu, J. C., and Chung, C. S., *Appl. Catal.* **18,** 295 (1985).
36. Newsome, D. S., *Catal. Rev. Sci. Eng.* **21,** 275 (1980).